

PALAIOS, 2019, v. 34, 515–541 Research Article DOI: http://dx.doi.org/10.2110/palo.2019.050



TAPHONOMY OF THE LOWER JURASSIC KONSERVAT-LAGERSTÄTTE AT YA HA TINDA (ALBERTA, CANADA) AND ITS SIGNIFICANCE FOR EXCEPTIONAL FOSSIL PRESERVATION DURING OCEANIC ANOXIC EVENTS

A.D. MUSCENTE, ^{1,2} ROWAN C. MARTINDALE, ² JAMES D. SCHIFFBAUER, ^{3,4} ABBY L. CREIGHTON, ² AND BROOKE A. BOGAN ² Department of Geology, Cornell College, 600 First Street SW, Mount Vernon, Iowa, 52314, USA ² Department of Geological Sciences, Jackson School of Geosciences, The University of Texas at Austin, 2275 Speedway, Austin, Texas, 78712, USA ³ Department of Geological Sciences, University of Missouri, 101 Geological Sciences Building, Columbia, Missouri, 65211, USA ⁴X-ray Microanalysis Core Facility, University of Missouri, 1 Geological Sciences Building, Columbia, Missouri, 65211, USA email: dmuscente@cornellcollege.edu

ABSTRACT: Konservat-Lagerstätten provide the most complete snapshots of ancient organisms and communities in the fossil record. In the Mesozoic, these deposits are rarely found in marine facies outside Oceanic Anoxic Event (OAE) intervals, suggesting that OAEs set the stage for exceptional fossil preservation. Although anoxia does not guarantee survival of non-biomineralized tissues or articulated skeletons, other OAE phenomena may promote their conservation. Here, we test this hypothesis with a taphonomic analysis of the Konservat-Lagerstätte in the black shales and siltstones of the Jurassic Fernie Formation at Ya Ha Tinda (Alberta, Canada). This deposit contains crustacean cuticles, coleoid gladii with ink sacs and mantle tissues, and articulated skeletons of fish, crinoids, and ichthyosaurs. The fossils were preserved in the Pliensbachian and Toarcian (Early Jurassic) when euxinic conditions were common in the area, in part, due to the \sim 183 Ma Toarcian OAE. Some of the fossils contain carbonaceous material, but the majority consists of apatite minerals, and phosphatic gladii demonstrate that some animals were preserved through secondary phosphate mineralization. Phosphatization generally occurs within phosphate-rich sediment, but oceanic anoxia causes sediment to release phosphorus and prevents animals from colonizing seafloor habitats. Accordingly, we propose that the animals were preserved during brief episodes of bottom water oxia and/or dysoxia, when the environment would have been most favorable to benthic communities and phosphate mineralization. In this setting, phosphatization may have been fueled by phosphate delivery from continental weathering in response to climatic warming, ocean upwelling of eutrophic water, and/or nutrient trapping by anoxia in the basin.

INTRODUCTION

The majority of the Phanerozoic fossil record consists of isolated shells, bones, teeth, and other skeletal materials. These fossils of biomineralizing organisms, however, represent only a fraction of the total biodiversity of life (Conway Morris 1986; Valentine 1989; Sperling 2017). Certain deposits-known as Konservat-Lagerstätten-have received special attention owing to their 'exceptionally preserved' fossils of non-biomineralized ('soft') tissues and/or articulated multi-element skeletons (Seilacher 1970; Allison and Briggs 1993; Muscente et al. 2017b). Because Konservat-Lagerstätten contain remains of entirely soft-bodied organisms in addition to skeletal fossils, they provide some of the most complete snapshots of ancient organisms and communities. Nevertheless, these exceptional deposits are scarce, as multi-element skeletons and non-biomineralized body parts are rapidly disarticulated, degraded, and destroyed in most environments by physical processes and post-mortem decay. Konservat-Lagerstätten are formed in rare circumstances where bodies survive degradation long enough to become buried in sediment, and in cases of soft tissue preservation, transformed into recalcitrant materials and/or minerals that can persist over geologic timescales (Briggs 2003). These circumstances arise in response to a combination of local, regional, and global phenomena. Local and regional factors that affect the likelihood of exceptional fossil preservation include sediment composition (Anderson et al. 2018), sedimentation rate, water circulation, topography, and local and regional climate (Allison and Briggs 1993; Briggs 2003). While their role

remains unclear, global phenomena may affect diagenetic conditions (Butterfield 1995), seawater chemistry (Gaines and Droser 2010; Gaines et al. 2012b), and the presence of geobiological agents, like sediment-mixing animals and microbial mats that affect scavenging and geochemical gradients (Schiffbauer et al. 2014b; Muscente et al. 2015a). Although these possibilities remain a subject of debate (Pickerill 1994; Butterfield 2012; Gaines et al. 2012a), oxygenation may represent the most significant control on the geographic and stratigraphic distribution of Konservat-Lagerstätten, as the availability of oxygen affects most (if not all) of the other phenomena (Muscente et al. 2017b).

Investigating exceptionally preserved fossils from Oceanic Anoxic Events (OAEs)—brief (<1 Ma) episodes of global or regional expansion of the oxygen minimum zone in the ocean (Schlanger and Jenkyns 1976; Jenkyns 1988, 2010; Takashima et al. 2006)—may help address this issue. Most marine Konservat-Lagerstätten occur in the Precambrian and lower Paleozoic, suggesting that conditions conducive to exceptional preservation declined in open marine settings during the early Paleozoic (Muscente et al. 2017b), likely in response to ocean oxygenation and compounded by the rise of bioturbation (Sperling et al. 2015; Tarhan et al. 2015). Subsequently, exceptional preservation rarely occurred in open marine settings (Muscente et al. 2017b), except during OAEs in the Early Jurassic (Röhl et al. 2001; Ansorge 2003; Williams et al. 2015; Martindale et al. 2017) and middle Cretaceous (Feldmann et al. 1999; Ifrim et al. 2007; Fuchs et al. 2008; Martill et al. 2011; Klug et al. 2012), when a number of

Published Online: November 2019

Copyright © 2019, SEPM (Society for Sedimentary Geology) 0883-1351/19/034-515

notable Konservat-Lagerstätten were preserved in such environments. At face value, the number and distribution of these deposits suggest that OAEs may lead to exceptional preservation (Seilacher et al. 1985; Allison 1988b; Allison and Briggs 1993; Martindale et al. 2017). Taphonomic experiments, however, show that anoxia does not guarantee the conservation of non-biomineralized tissues or the preservation of articulated skeletons held together by integuments, as anaerobic metabolic processes can degrade soft tissue as rapidly as aerobic decay (Allison 1988c). Thus, Konservat-Lagerstätten in OAE intervals may reflect the effects of other environmental phenomena. For example, exceptional fossil preservation may occur on the edges of anoxic environments, where redox boundaries create geochemical gradients conducive to fossil mineralization (Muscente et al. 2015a). Sedimentation also affects the burial rates of organisms, and therefore, their exposure to various aerobic and anaerobic processes of degradation (Schiffbauer et al. 2014b). Ergo, exceptional preservation may occur where anoxia intersects and complements other phenomena that limit degradation and promote mineralization of tissues (Muscente et al. 2017b).

The Toarcian OAE (\sim 183 Ma) provides an opportunity for exploring the relationship between oceanic anoxia and exceptional fossil preservation. This event involved climatic warming and oceanographic change, which may have been caused by (1) the emplacement of the Karoo-Ferrar large igneous province and the onset of massive volcanism (Pálfy and Smith 2000; Moulin et al. 2017); (2) thermal dissociation of gas hydrate and release of methane from continental margin sediments (Hesselbo et al. 2000); (3) destabilization of terrestrial organic matter and coal (McElwain et al. 2005; Pieńkowski et al. 2016); and/or (4) other processes or combinations of factors (Beerling and Brentnall 2007; Svensen et al. 2007; Them et al. 2017a). Regardless of its origin, the event involved the rise of protracted anoxic conditions and the deposition of black shales and other organic-rich rocks in marine basins around the world (Jenkyns 1988, 2010; Them et al. 2018). These rocks have a geochemical signature—a carbon isotope excursion produced by a major perturbation in the carbon cycle allowing for global correlation of the strata (Al-Suwaidi et al. 2010; Caruthers et al. 2011; Gröcke et al. 2011; Suan et al. 2011; Kemp and Izumi 2014; Them et al. 2017a). The rocks also contain fossils that provide evidence for pelagic and benthic extinctions of ammonites, bivalves, brachiopods, corals, fish, foraminifers, and radiolarians during the OAE (Little and Benton 1995; Lathuilière and Marchal 2009; Caruthers et al. 2014; Caswell and Coe 2014; Danise et al. 2015; Martindale and Aberhan 2017). Broadly contemporaneous with the OAE, several open marine Konservat-Lagerstätten were deposited, including those of the Posidonia Shale at various sites (primarily) in Germany (Seilacher 1990; Röhl et al. 2001), the Beacon Limestone Formation at the Strawberry Bank site in the United Kingdom (Williams et al. 2015), and the lower Fernie Formation at Ya Ha Tinda Ranch in Alberta, Canada (Martindale et al. 2017).

The black shales and organic-rich (shaley) siltstones of the Red Deer and Poker Chip Shale members of the Fernie Formation at Ya Ha Tinda Ranch contain the only Konservat-Lagerstätte reported, thus far, from the Jurassic of North America as well as the only Pliensbachian-Toarcian Lagerstätte known outside of Europe (Martindale et al. 2017; Muscente et al. 2017b). These strata contain exceptionally preserved animals at multiple levels, but the preservational pathways of these fossils have not been described in detail (Martindale et al. 2017). Exceptionally preserved Ya Ha Tinda fossils include crustacean (shrimp and lobster) cuticles (Feldmann and Copeland 1988; Schweigert 2003); coleoid gladii with ink sacs and mantle muscle tissues (Hall 1985; Marroquín et al. 2018); and articulated skeletons of crinoids (Hall 1991), fish (Maxwell and Martindale 2017), and ichthyosaurs (Hall et al. 1998). Additional fossils include ammonites, belemnites, bivalves, gastropods, linguliformean brachiopods, rhynchonellid brachiopods, coccolithophores, wood, a dinosaur bone, and various trace fossils, including coprolites (Hall et al. 1998; Martindale and Aberhan 2017; Martindale et al. 2017). Ammonite biostratigraphy, carbon isotope chemostratigraphy, and radiometric dates from ashes constrain the chronology of events at Ya Ha Tinda (Hall et al. 1998, 2004; Hall 2006; Martindale et al. 2017; Them et al. 2017a, 2018). The fossils of the Konservat-Lagerstätte occur from the upper Pliensbachian (late *kumae* ammonite zone) to the middle Toarcian (*planulata* ammonite zone), which corresponds to the *margaritatus* through *bifrons* European ammonite zones (Martindale et al. 2017). Geochemical redox proxies suggest that euxinia (anoxia with a high concentration of free hydrogen sulfide in the water) was common in the depositional environment during the Early Jurassic (Them et al. 2018). In this context, a taphonomic analysis of the Ya Ha Tinda Lagerstätte may shed light on the relationship between OAEs, anoxia, and exceptional fossil preservation.

In this paper, we investigate the origin of exceptionally preserved fossils in the Ya Ha Tinda Lagerstätte with emphasis on its potential relationship with oceanic anoxia. Specifically, our work utilizes data collected with scanning electron microscopy (SEM) and energy-dispersive X-ray spectroscopy (EDS) to describe the compositions, mineralogies, and ultrastructures of the fossils (Orr et al. 2002, 2009; Muscente and Xiao 2015b; Muscente et al. 2016). By studying the paragenesis of the minerals and their cross-cutting relationships, we reconstruct the preservational pathways and paleoenvironments of the fossils, rooting our analysis in taphonomic, geomicrobiological, and oceanographic processes (Muscente et al. 2017b). Using these results, we propose a model that links fossil mineralization at Ya Ha Tinda to regional phenomena brought about by oceanic anoxia. In addition, we discuss the significance of our work for the taphonomy of similar Mesozoic deposits (e.g., the Posidonia Shale). Altogether, our investigation reconciles field- and laboratory-based analyses of exceptional fossil preservation, providing insights into the stratigraphic and geographic distribution of Konservat-Lagerstätten and highlighting the potential for future discoveries in OAE intervals.

GEOLOGIC SETTING

Western Alberta was located on the eastern edge of the Panthalassa Ocean in the Early Jurassic (Fig. 1). During this time, the Fernie Formation was deposited on a sediment-starved platform (gently sloping shelf to basin) along a passive margin of the Western Canada Sedimentary Basin during an epicratonic phase in its tectonic history (Hall et al. 1998). The Fernie Formation now outcrops in the foothills of the Canadian Rocky Mountains (Hall 1987, 2006; Hall et al. 1998, 2004). Although its exposure on the surface is generally poor, the unit persists northward and eastward in the subsurface (Hall et al. 1998). Ammonite biostratigraphy indicates that the unit spans from the Pliensbachian Stage to the Aalenian Stage of the Lower Jurassic (Hall 1987; Pálfy and Smith 2000; Hall 2006). North American ammonite zones have been correlated to the ammonite zones from northwest Europe, allowing for relative dating through intraand inter-regional correlations.

In the study area northwest of Calgary at Ya Ha Tinda Ranch near Banff National Park, the Fernie Formation outcrops in sections measured along Scalp Creek (Tyrrell Museum of Palaeontology, or TMP, Locality L2430), Bighorn Creek (TMP Locality L2429), and an eastern tributary (TMP Locality L2428) of Bighorn Creek (Hall 1987, 2006; Hall et al. 1998, 2004; Martindale and Aberhan 2017; Martindale et al. 2017; Them et al. 2017a). As the site with the best exposure, the 'East Tributary' section has generally received the most attention for biostratigraphy, chemostratigraphy, and paleobiology (Martindale and Aberhan 2017; Martindale et al. 2017; Them et al. 2017a, 2018). As all of these outcrops occur on land owned by Parks Canada, they are protected under the Canadian National Parks Act, and their precise locations cannot be disclosed. All fossils and geological samples, which were acquired for this study, were collected under a Parks Canada collection and research permit (#YHTR-2014-16156) and fossil excavation permits from the Alberta Government (RTMP Permits: #13-058, #14-009, #15-019, #16-063, #17-048, and #18-072).

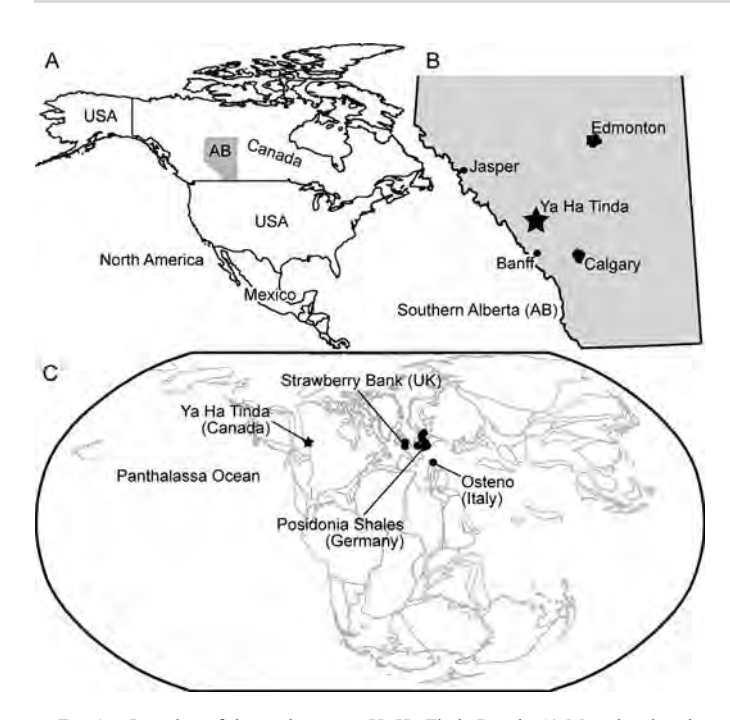


Fig. 1.—Location of the study area at Ya Ha Tinda Ranch. A) Map showing the position of Alberta (AB), Canada, within North America. B) Map of southern Alberta with location of Ya Ha Tinda and major cities. C) Map of the world around 180 Ma showing paleogeographic locations of Ya Ha Tinda and other Early Jurassic Konservat-Lagerstätten (Muscente et al. 2017b). The paleogeographic locations of the points at 180 Ma were estimated, based on their present coordinates, using the global plate motion model for the Phanerozoic produced by Wright et al. (2013) and the map was rendered in GPlates (Qin et al. 2012).

At Ya Ha Tinda, the Fernie Formation overlies the Middle Triassic siltstones of the Sulphur Mountain Formation (Fig. 2). The Lower Jurassic Fernie Formation includes the Red Deer and Poker Chip Shale members (Hall et al. 2004; Hall 2006). The Red Deer Member consists of gray to black platy calcareous shales interbedded with fine siltstones and black limestones. Some beds in this unit contain shell pavements, trace fossils, and evidence of bioturbation (Figs. 2, 3A, 3Q), in addition to lath-shaped barite (Martindale and Aberhan 2017; Martindale et al. 2017; Them et al. 2017a), which may be a pseudomorph of gypsum, given its crystal morphology, habit, and millimetric size (Fig. 2, Scalp Creek). The shales and siltstones of this member are typically well cemented, and carbonate concretions are somewhat common. In contrast to the Red Deer Member, the overlying Poker Chip Shale Member is mainly comprised of black calcareous shales and mudstones, which are relatively fine-grained, poorly cemented, and fissile. In addition, the Poker Chip Shale Member generally has higher values of total organic carbon (TOC), measured in weight percent (wt%). Its TOC values sometimes reach 18.5 wt% (Riediger 2002) but generally range between 1 and 7 wt% (Them et al. 2017a). The quality of outcrop declines toward the top of the Poker Chip Shale Member, and exposure becomes spotty. The Poker Chip Shale is overlain by the Highwood Member, which is about 20 m thick at Ya Ha Tinda, and composed of gray, rusty, and yellow shales containing calcareous concretions, phosphatic pebbles, fragmentary belemnites, and abundant gypsum and goethite (Hall et al. 1998, 2004). Above the Highwood Member, the sections terminate with gray shales ('gray beds') lacking formal designations.

Overall, the sedimentary succession of the Fernie Formation at Ya Ha Tinda Ranch spans from the Pliensbachian to the Middle Jurassic. A bentonite in the lower part of the Red Deer Member in the East Tributary section (~1 m above its boundary with the Sulphur Mountain Formation)

has produced a zircon with a U-Pb radiometric age of 188.3 ± 1.5 Ma (Hall et al. 2004). Additional ages of 188.58±0.17 Ma and 185.49±0.16 Ma have been reported from the lower part of the Red Deer Member in this section (Them et al. 2017b, 2018). The ammonite biostratigraphy of the East Tributary section places the Pliensbachian/Toarcian boundary in the Red Deer Member, roughly 1 m below its contact with the Poker Chip Shale Member (Them et al. 2017a). Around this contact, the organic carbon isotope ($\delta^{13}C_{org}$) profile of the section precipitously drops from -27 to -31% before gradually recovering over five meters toward the top of the section (Fig. 2). This trend represents the local signature of the global perturbation in the carbon cycle associated with the Toarcian OAE (Them et al. 2017a) and can be correlated with the carbon isotope excursion measured in Toarcian rocks around the world (Al-Suwaidi et al. 2010; Caruthers et al. 2011; Gröcke et al. 2011; Suan et al. 2011; Kemp and Izumi 2014). The appearance of the excursion coincides with evidence for fossil turnover and diminution, consistent with an extinction event (Martindale and Aberhan 2017). Although the quality of outcrop declines toward the top of the Poker Chip Shale Member, its ammonites indicate that the unit, by and large, consists of Toarcian strata (Them et al. 2017a). The Highwood Member at Ya Ha Tinda has only yielded rare ammonites (Hall 2006), but elsewhere in Alberta, it contains fossils of Middle Jurassic age (Hall et al. 2004). In addition, bentonites in this unit at Bighorn Creek and East Tributary have yielded zircons with radiometric ages of 173 Ma and 166.6±0.2 Ma, which are also consistent with the Middle Jurassic (Hall et al. 2004). Moreover, a bentonite in the 'gray beds' at East Tributary has produced a zircon with an age of 165.4±0.3 Ma (Hall et al. 2004). Thus, all data support the interpretation that the Red Deer and Poker Chip Shale members record the Pliensbachian-Toarcian transition and the Toarcian OAE.

MATERIAL, EQUIPMENT, AND METHODS

Material and Preparation

Fossils were collected from the Konservat-Lagerstätte in the Fernie Formation at Ya Ha Tinda by the authors and others over the course of many years of sampling (Hall 1987; Martindale and Aberhan 2017; Martindale et al. 2017), resulting in the accumulation of, at least, 1188 specimens of identifiable fossil material (Table 1). All specimens illustrated in this study are curated and reposited in the Royal Tyrrell Museum of Palaeontology in Drumheller, Alberta, Canada. For each of four groups of fossils-shelly fossils, fish, crustaceans, and coleoidsthree or more specimens of appropriate size (dimensions no more than 6 cm × 6 cm × 2 cm) were photographed according to standard reflected light techniques and analyzed with scanning electron microscopy (SEM) and energy-dispersive X-ray spectroscopy (EDS). Fossils were also examined under ultraviolet light. A number of specimens (indicated in text) were photographed under directional illumination and/or were coated with ammonium chloride salt sublimate in order to increase the contrast of fine details (Feldmann 1989). This study utilized two different variable pressure SEM systems, in which the specimen chamber is held at lowpressures that allow for the ionization and electrical conduction of surface charge by chamber gases. Consequently, the imaging analyses did not require deposition of conductive coating onto the curated specimens. To minimize charging of non-coated surfaces during electron imaging, we wrapped all rock pieces in aluminum or copper foil tape with only the fossils exposed, and mounted the samples in the chamber so that the foil was connected to the stage, thereby grounding electrical charge on the sample surface (Orr et al. 2002).

Electron Imaging

We employed SEM systems housed in the Jackson School of Geoscience in the University of Texas at Austin (UT Austin) and the X-

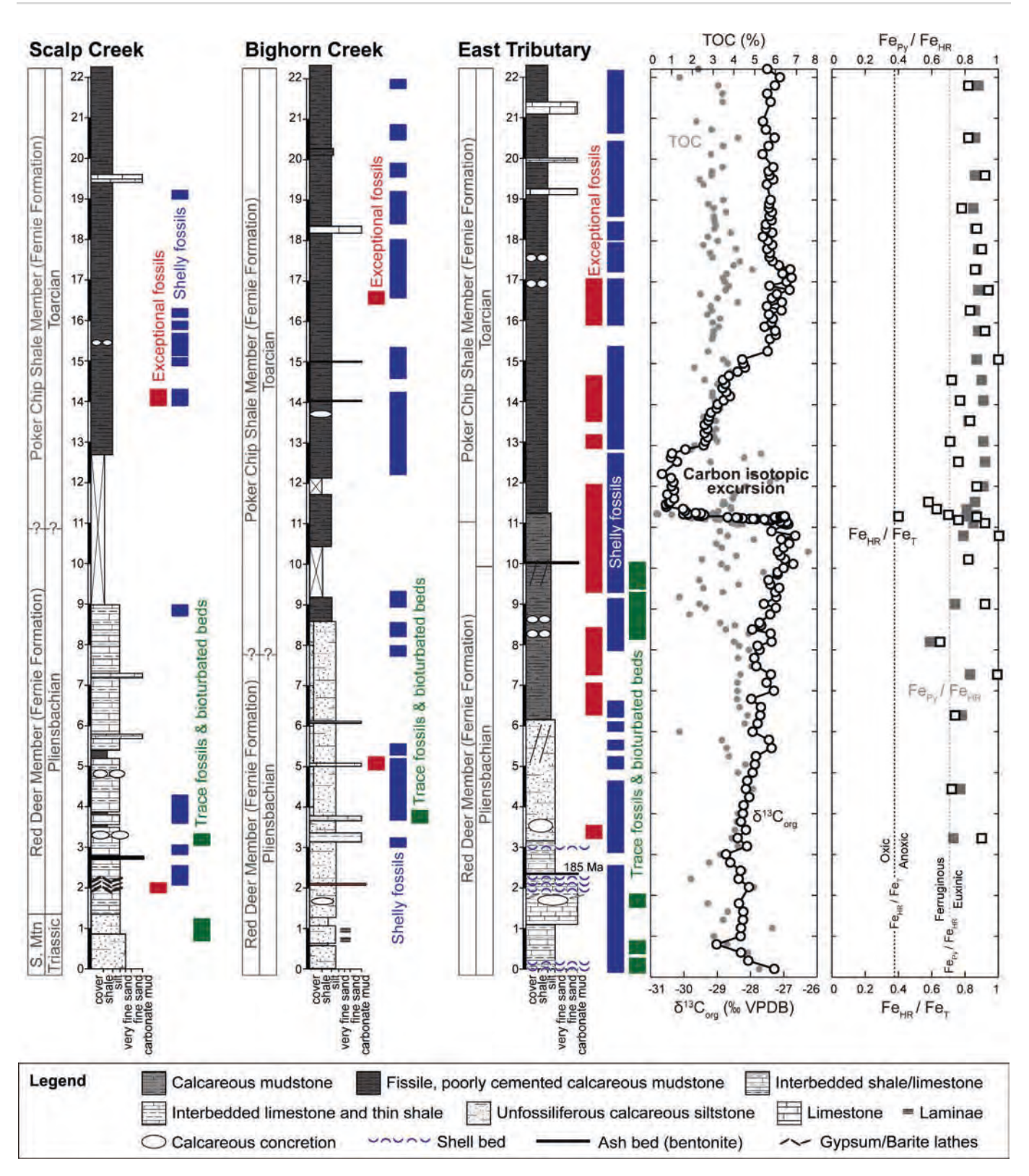


Fig. 2.—Stratigraphic columns of three Lagerstätte-bearing sections of the Fernie Formation exposed at Ya Ha Tinda Ranch. The sections were measured along Scalp Creek (TMP Locality L2430), Bighorn Creek (TMP Locality L2429), and an eastern tributary of Bighorn Creek (TMP Locality L2428). Columns illustrate the stratigraphic distributions of fossils and bioturbation (Martindale and Aberhan 2017; Martindale et al. 2017) and the lithostratigraphy and chronostratigraphy of the sections (Them et al. 2017a). The organic carbon isotope ($\delta^{13}C_{org}$), total organic carbon (TOC) values in weight percent, and iron speciation profiles of the East Tributary section are also shown (Them et al. 2017a, 2018). Fossils include exceptional specimens (arthropod carapaces, coleoid gladii, and articulated fish, crinoids, and ichthyosaurs); shelly fossils (ammonites, bivalves, brachiopods, belemnites, and isolated crinoid ossicles); and traces like *Diplocraterion*, *Thalassinoides*, *Arenicolites*, *Rhizocorallium*, and *Rusophycus*. Iron speciation data are presented as ratios of pyrite iron (Fe_{Py}), highly reactive iron (Fe_{HR}), and total iron (Fe_T), allowing for differentiation of seemingly oxic, ferruginous anoxic, and euxinic anoxic conditions.

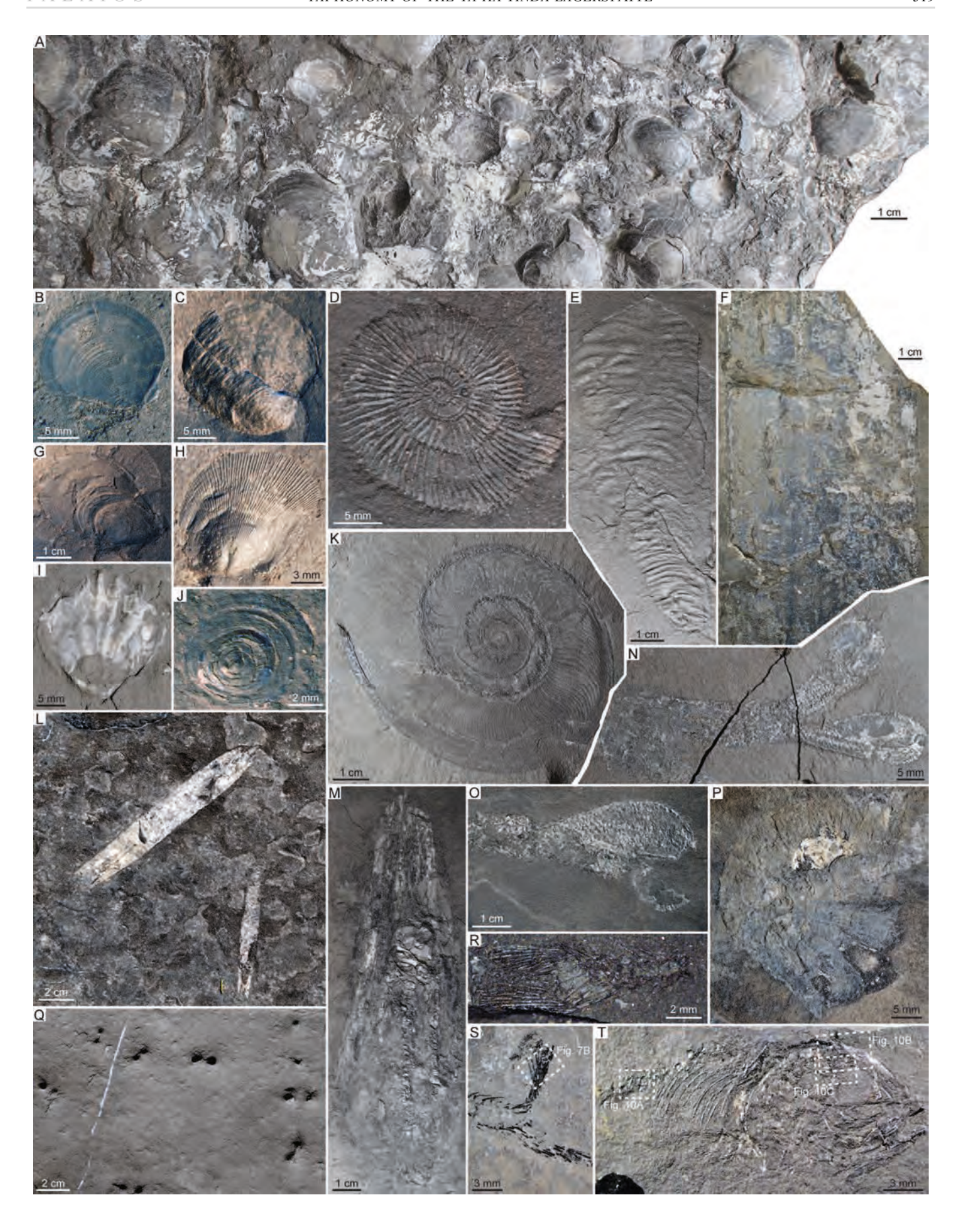


Table 1.—Summary of the Fernie Formation fossils from Ya Ha Tinda Ranch curated at the Royal Tyrrell Museum of Palaeontology. Fossils are divided among broad, identifiable taxonomic groups as well as by age, lithology, and collection site (i.e., section). Raw numbers listed with the proportion of total fossil specimens in brackets. Data downloaded from the RTMP collections database on August 2018 and revised for consistency (e.g., sites were synonymized and ages were added based on stratigraphic information in field notes).

Taxon	All specimens	Geologic stages		Lithostr	atigraphic units	Sections and localities			
		Pliensbachian	Toarcian	Red Deer	Poker Chip Shale	Bighorn Creek	Scalp Creek	East Tributary	
Ammonoidea	683 (0.57)	96 (0.08)	479 (0.4)	145 (0.12)	432 (0.36)	256 (0.22)	107 (0.09)	320 (0.27)	
Bivalvia	231 (0.19)	18 (0.02)	179 (0.15)	24 (0.02)	175 (0.15)	16 (0.01)	84 (0.07)	127 (0.11)	
Unidentified	90 (0.07)	44 (0.04)	9 (0.01)	54 (0.04)	7 (0.01)	15 (0.01)	2 (0)	73 (0.06)	
"Lobsters"	70 (0.06)	37 (0.03)	13 (0.01)	70 (0.06)	0 (0)	0 (0)	1 (0)	69 (0.06)	
Brachiopoda	30 (0.03)	5 (0)	6 (0.01)	9 (0.01)	4 (0)	3 (0)	19 (0.02)	8 (0.01)	
Coleoidea	27 (0.02)	9 (0.01)	15 (0.01)	17 (0.01)	9 (0.01)	3 (0)	1 (0)	23 (0.02)	
"Fish"	16 (0.01)	5 (0)	9 (0.01)	6 (0.01)	9 (0.01)	2 (0)	3 (0)	11 (0.01)	
Crustacea	13 (0.01)	3 (0)	9 (0.01)	5 (0)	8 (0.01)	0 (0)	0 (0)	13 (0.01)	
Ichthyosauria	9 (0.01)	3 (0)	0 (0)	3 (0)	0 (0)	6 (0.01)	2 (0)	1 (0)	
Belemnitida	7 (0.01)	2 (0)	1 (0)	4 (0)	0 (0)	0 (0)	3 (0)	4 (0)	
Crinoidea	5 (0)	3 (0)	1 (0)	4 (0)	0 (0)	1 (0)	1 (0)	2 (0)	
Vertebrata	3 (0)	1 (0)	2 (0)	1 (0)	2 (0)	0 (0)	0 (0)	3 (0)	
Plantae	2 (0)	0 (0)	1 (0)	2 (0)	0 (0)	0 (0)	1 (0)	1 (0)	
Gastropoda	1 (0)	0 (0)	0 (0)	0 (0)	0 (0)	1 (0)	0 (0)	0 (0)	
"Coprolites"	1 (0)	0 (0)	1 (0)	0 (0)	1 (0)	0 (0)	0 (0)	1 (0)	
Total	1188 (1)	226 (0.19)	725 (0.61)	344 (0.29)	647 (0.54)	303 (0.26)	224 (0.19)	656 (0.55)	

ray Microanalysis Core at the University of Missouri (Mizzou). The UT Austin system is a JEOL 6490LV microscope with tungsten hairpin filament electron gun; pole piece backscattered electron (BSE) solid state detector (SSD) with two diodes; Everhart-Thornley-type secondary electron (SE) detector; and EDAX Genesis EDS detector. At UT Austin, SEM images were acquired with an electron beam at an accelerating voltage of 20 keV, spot size of 50 nm, and working distance of 10 mm-15 mm. The Mizzou SEM system used is a Zeiss Sigma 500VP with a field emission electron gun; a 5-segment high-definition SSD BSE detector (HDBSD); a cascade current low vacuum secondary electron detector (C2D); an Atlas 5 correlative microscopy workflow system; and dual, coplanar Bruker XFlash 6|30 EDS units. At Mizzou, SEM imaging was conducted with both the C2D for secondary (topographic) images and the HDBSD for backscattered (compositional) images. All imaging on this system was conducted at ~15 mm working distance (variability from sample topography) in high current mode (40 nA) with a 20 keV beam accelerating voltage and 60 µm aperture.

For each BSE image, the operating conditions and imaging mode were selected in order to optimally visualize specific sample properties, such as compositional heterogeneity, surficial topography, and subsurficial mass-thickness variations (see Muscente and Xiao 2015b for a review of the mechanisms of contrast formation in BSE imaging). The BSE images were

variably acquired with the compositional and topographic imaging modes (Muscente and Xiao 2015b). In general, the compositional imaging mode produces BSE images with optimal compositional (atomic number, or Z) contrast by digitally adding signals collected by the two SSD diodes. Conversely, the topographic imaging mode produces BSE images with optimal topographic relief contrast by digitally subtracting signals from the different SSD diodes and combinations of diodes. In this case, contrast reflects topographic variations on the surface of the sample affecting BSE emission and detection. We primarily focus on BSE images from the compositional imaging mode, as they best illustrate the various minerals and materials present in the fossils. At UT Austin, high-resolution composite BSE images of specimens larger than the imaging area at the lowest magnification level (horizontal field width around 4.5 mm) were assembled from multiple high-magnification images acquired with the same operating conditions (focus setting, brightness, contrast, dwell time, probe spot diameter, working distance, imaging mode, and accelerating voltage). The brightness and contrast of some BSE images were digitally adjusted with Adobe Photoshop to produce publication-quality figures (Goldstein et al. 2003). Enhancements were applied equally across BSE images, and did not introduce signal biases. Comparison with the original images confirms that digital processing did not alter relative contrast patterns. At Mizzou, large image mosaics of both BSE and SE signals were

Table 2.—Summary of EDS data for the various materials (rows) in the Fernie Formation fossils from Ya Ha Tinda Ranch. Numbers outside parentheses are mean atomic percentages for the elemental peaks (columns); numbers inside parentheses are the associated standard error values. Values were calculated from point spectra of number (n) taken from all of the specimens analyzed with EDS. Table excludes values for elements with mean atomic percentages less than 1.

	n	AlK	BaL	CaK	CK	FeK	OK	PK	SiK	SK	ZnK
Aluminosilicate veneer	6	16.36 (0.3)	-	-	17.22 (0.57)	-	46.2 (0.58)	-	18.18 (0.25)	-	-
Barite	20	1.56 (0.3)	16.65 (0.59)	1.42 (0.23)	18.39 (1.23)	-	42.93 (1.22)	-	3.61 (0.59)	16.34 (0.5)	-
Calcareous shell	3	1.1 (0.26)	-	26.35 (0.46)	12.22 (1.38)	-	58.65 (1.37)	-	1.69 (0.37)	-	-
Calcite	8	-	-	22.82 (3.73)	22.47 (1.44)	-	41.04 (3.09)	1.05 (0.21)	1.46 (0.22)	-	-
Carbonaceous material	19	-	-	9.81 (0.76)	61.46 (2.56)	-	16.12 (1.45)	5.44 (0.43)	1.32 (0.4)	1.81 (0.21)	-
Gypsum	2	2.23 (0.51)	-	14.11 (1.06)	-	1.51 (0.42)	62.35 (0.9)	-	3.37 (0.43)	15.82 (0.05)	-
Matrix	23	6.74 (0.88)	-	4.34 (0.74)	19.16 (1.19)	-	41.12 (1.4)	-	24.56 (1.19)	-	-
Phosphatic grains	4	-	-	28.9 (3.8)	20.34 (2.33)	-	24.9 (7.78)	17.88 (1.61)	1.45 (0.56)	-	-
Phosphatic material	11	1.07 (0.12)	-	21.57 (0.93)	25.62 (1.54)	-	33.81 (1.86)	11.52 (0.65)	1.38 (0.14)	-	-
Pyritized shell	2	2.83 (0.71)	-	3.6 (0.14)	-	20.44 (0.04)	22.43 (1.53)	2.55 (0.58)	3.8 (0.57)	44.37 (0.23)	-
Sphalerite	8	2.08 (0.38)	-	1.65 (0.34)	33.36 (1.29)	-	12.6 (2.19)	-	3.77 (0.78)	22.13 (1.8)	22.7 (2.2

assembled from full fossil surfaces according to an automated process using the Atlas 5 workflow. Any digital adjustments or enhancements were applied equally within the Atlas 5 software interface.

Elemental Analysis

The elemental maps and concentration data in this study (Table 2) were collected using both the EDAX Genesis EDS detector on the JEOL 6490LV system (UT Austin) and the dual Bruker XFlash detectors on the Zeiss Sigma 500 VP system (Mizzou). On the EDAX, elemental maps and point spectra analyses of specimens were conducted at an electron accelerating voltage of 20 keV, 12-15 mm working distances, for live times of 400 to 1200 seconds (s), and with X-ray count rates of 3000 counts/s to 6000 counts/s, depending on the sample. Elemental peaks of spectra were identified and quantified using the Genesis Spectrum Software (version 6.43) by EDAX. The point spectra were used to produce semi-quantitative measurements of elemental concentrationsreported in weight percent and atomic percent-for elements found at appreciable levels in the minerals, materials, and substrates of the fossils (Muscente and Xiao 2015b). To ensure reproducibility, multiple measurements were taken for each mineral, material, or substrate, and the mean atomic percentages of those measurements were calculated. The mean atomic percentages, or the average numbers of atoms of each element, provide stochiometric ratios for determining the identities of some minerals. On the Zeiss Sigma system, EDS maps were collected for 480 s live time using both detectors in tandem, with count rates >150kilocounts/s, beam accelerating voltage of 20 keV and 40 nA current, ~15 mm working distance, and with a 120 µm aperture for greater signal.

RESULTS

Shelly Fossils

The most common fossils in the Red Deer and Poker Chip Shale members are ammonites (57%) and bivalves (19%); brachiopods (3%), belemnites (1%), crinoids (<1%), and gastropods (<1%) also make up the shelly fauna (Table 1; Fig. 3A–3I, 3K, 3L; Martindale and Aberhan 2017). The topographic relief of these fossils is generally low (Fig. 4). Some of the fossils react when treated with hydrochloric acid, and combined BSE and EDS analysis shows that they consist of calcium carbonate in the form calcite (Fig. 4). Although framboidal and euhedral crystals of iron sulfide (pyrite) occur in some of the shelly fossils and surrounding matrix (Fig. 4B), few of the originally aragonitic or calcitic shells have been replaced by

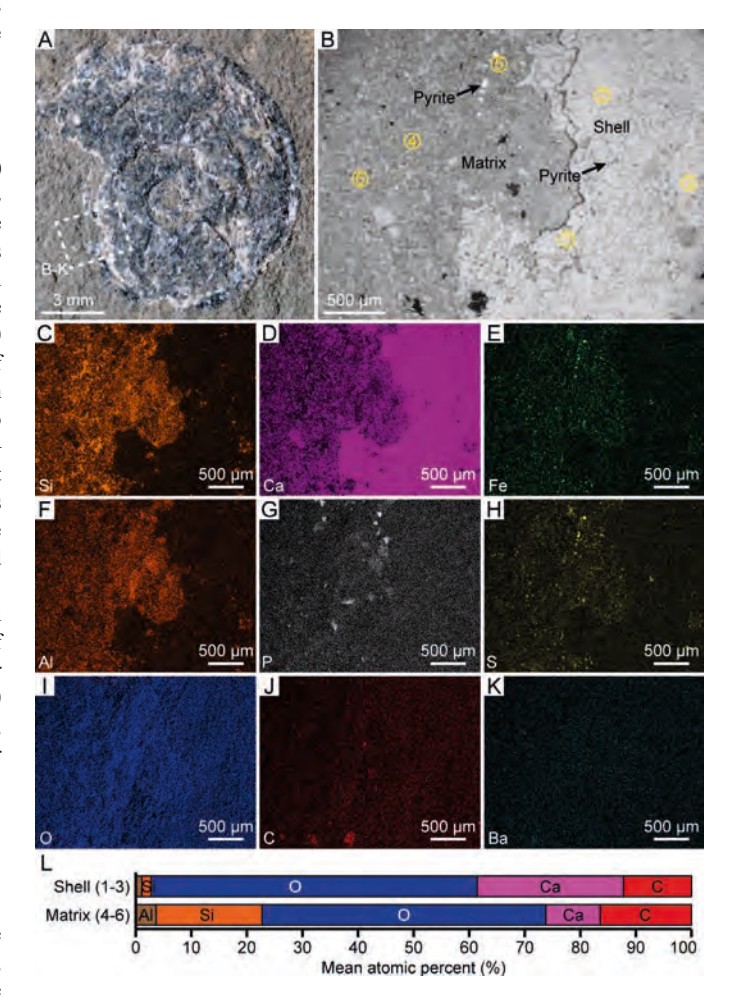


Fig. 4.—Ammonite from Red Deer Member, East Tributary (TMP2018.024.0063). A) Reflected-light image. B) BSE image acquired with the compositional imaging mode. Numbered circles enclose points, which were analyzed with EDS to collect semi-quantitative elemental concentration data. Arrows point to pyrite framboids and euhedral crystals associated with the fossil. C–K) EDS elemental maps of the view in B. L) Bar plot illustrating elemental concentration data, which are reported as mean (normalized) atomic percentages. Numbers in parentheses correspond to points in the BSE image.

pyrite (Martindale et al. 2017). In many cases, their calcium carbonate has been dissolved, leaving behind only impressions that do not differ from the matrix in terms of composition or mineralogy.

The shells of the linguliformean brachiopod Discinisca are generally phosphatic in composition (Figs. 3J, 5). Combined BSE and EDS analysis demonstrates that these shells retain their exterior morphology (Fig. 5B), contain higher concentrations of calcium and phosphorus than the surrounding matrix (Fig. 5C, 5I-5N), and are associated with a number of minerals (Fig. 5C-5H). These minerals occur sporadically throughout the rock, but in general, are most common near the fossils. Semiquantitative measurements of the elemental concentrations and stoichiometric ratios of these minerals (Fig. 6; Table 2) allow for identification of pyrite, barium sulfate (barite), and calcium sulfate (gypsum). In rare cases, linguliformean shells are secondarily mineralized with pyrite (Fig. 5C, 5I-5N). Whereas the pyrite occurs within the shells of these fossils (Fig. 5D, 5O-T), the barite and gypsum cover the exterior surfaces of the phosphatic material (Fig. 5G, 5F, 5U-5Z). The barite typically consists of large (>5 um diameter) euhedral crystals (Fig. 5E). Gypsum, conversely, occurs as aggregates of flat crystal sheets (Fig. 5F).

Fish

Leptolepiform and saurichthyiform teleost fish are rare (1%) among the fossils from the Fernie Formation (Table 1). They include isolated bones and variably articulated skeletons with vertebrae, ribs, skulls, scales, fins, and gill arches; identifiable genera include Leptolepis and Saurorhynchus (Figs. 3R-3T, 7-9; Maxwell and Martindale 2017). Thus far, there have been no discoveries of non-biomineralized tissues in the fish fossils, although delicate structures (e.g., gill arches) are well preserved (Fig. 9). Even in articulated specimens, the fish skeletons are generally flat with only minor topographic relief (Fig. 9). The skeletal elements are generally preserved as phosphatic materials with higher concentrations of calcium and phosphorus than the surrounding rock matrix (Figs. 7, 8). In some specimens (Fig. 3T), the fish skeletons are comprised of both phosphatic (Figs. 9A, 9B, 9D-9K, 9S-9Y, 10A, 10E-10K) and carbonaceous materials (Figs. 9A, 9C, 9D, 9L-9Y, 10B, 10L-10R), which are encrusted and surrounded by a number of accessory minerals (Figs. 9B, 9C, 9E-9K, 9S-9Y, 10B, 10C, 10L-10Y).

Elemental maps and semi-quantitative measurements of elemental concentrations and stoichiometric ratios (Fig. 10Z; Table 2) allow for the identification of the following accessory minerals in the fish fossils: aluminosilicate clays (Fig. 10B), pyrite (Fig. 9D), barite (Fig. 10B), and the zinc sulfide mineral, sphalerite (Fig. 10C). The aluminosilicate clays, which appear in EDS elemental maps as areas of relatively high Al, Fe, Mg, and O (but low K and Si) concentration with respect to the surrounding rock matrix (Fig. 10B, 10L-10R, 10Z), constitute thin veneers encrusting the carbonaceous and phosphatic materials. These veneers are most visible in places where the carbonaceous and/or phosphatic materials have been naturally and purposefully broken away from the rock, leaving Al-rich veneer layers exposed on top of the Alpoor matrix (Fig. 10B). Like the shells of the linguliformean brachiopods, the exterior surfaces of the fish skeletons are sometimes encrusted by barite (Fig. 8C, 8D, 8G-8R). The barite typically consists of large (>5 µm diameter) euhedral crystals, but in some places, appears bladed and tabular in morphology (Fig. 8E, 8F). Barite also occurs with sphalerite and pyrite as cement in the matrix around some fish (Figs. 9A, 9B, 9D, 10C). By and large, the pyrite occurs as small disseminated framboids in the surrounding rock (Fig. 10D). Elemental maps reveal high concentrations of iron and sulfur in some places around the fish, indicating that pyrite framboid abundance varies with proximity to the fossils (Fig. 9D, 9S-9Y). Despite the presence of framboidal pyrite, the fish contain no pyritized tissues.

Crustaceans

The Red Deer and Poker Chip Shale members contain fully and partially articulated shrimp and lobster (decapod crustacean) carapaces (Fig. 3N–3P), which are somewhat common (7%) among the fossils from the units (Table 1). These remains represent the exoskeletons or cuticles of the animals (Martindale et al. 2017), and there have been no reports of other types of tissues. Most of the decapod fossils are fragments of appendages (i.e., claws); shrimp are rare, and full lobster carapaces have only been reported below the Toarcian OAE carbon isotope excursion (Martindale et al. 2017). The vast majority of lobsters identified to date belong to two *Uncina* species (Family Uncinidae): *U. pacifica* and *U. ollerenshawi* (Feldmann and Copeland 1988; Schweigert 2003; Martindale et al. 2017).

The crustacean fossils have little topographic relief (Figs. 11-13). Combined BSE and EDS analysis illustrates that the crustaceans are preserved, like the fish and linguliformean brachiopods, as phosphatic and carbonaceous materials encrusted by accessory minerals (Figs. 11-13). The carbonaceous material is typically sparse, and the carapaces primarily consist of calcium phosphate (Fig. 11). Where fossils retain structures of morphological and ultrastructural ornamentation (e.g., bump or spikes), the structures are comprised of the phosphatic material (Figs. 11C, 11E-11K, 13B-13E, 13H-13N). In these cases, carbonaceous material may fill phosphatic molds (Fig. 11C) or occur as a continuous layer on top of the phosphatic material with ultrastructural ornamentation (Figs. 12C-12R, 13B-13F). The continuous layers of carbonaceous material contain phosphatic granules (Figs. 12D, 13G), tens of microns in scale, that resemble the ornamented phosphatic material in terms of relative Z-contrast (Fig. 13F) and elemental concentrations (Fig. 13V; Table 2). Elemental maps and semi-quantitative data from EDS show that the phosphatic and carbonaceous materials are associated with two minerals: barite and calcium carbonate (Figs. 11, 12C, 12D, 13B-13D, 13H-13N; Table 2). In both cases, the minerals are large euhedral crystals. Based on crystal morphology, the calcium carbonate mineral can be identified as calcite (Fig. 11D). Under reflected light, the calcite appears white or clear (Figs. 11B, 13B). Notably, the calcite occurs in thick crusts on the phosphatic and carbonaceous materials (Figs. 11D, 12C, 12D).

Coleoids

Coleoids make up a small percentage (2%) of the fossils in the Fernie Formation (Table 1). These specimens represent the gladii (Fig. 3M), or chitinous internal shells, of vampyropod (eight-armed) cephalopods (Marroquín et al. 2018). Many gladii retain growth lines (Fig. 14B) and ink sacs (Fig. 15); in rare cases, the gladii are preserved with mantle muscle tissues and evidence of muscle striations (Fig. 15; Marroquín et al. 2018). The gladius of one specimen (Fig. 14) was deposited and buried on top of the disarticulated ossicles of the crinoid *Seriocrinus subangularis* (Marroquín et al. 2018).

The gladii exhibit little topographic relief, except where they overlap crinoid ossicles (Fig. 14A–14E) and contain mantle and ink sac remains (Fig. 15A–15D). They mostly consist of apatite minerals, like the other exceptionally preserved fossils in the Lagerstätte (Figs. 14–17). Although the mantle remains are generally preserved as impressions in the rock (Fig. 15A, 15B, 15D), which are covered in places by carbonaceous matter (Fig. 15E, 15G–15N), they also contain phosphatic materials in some places (Fig. 16). The ink sacs likewise consist of numerous materials, but at their cores, they largely consist of apatite minerals (Fig. 15F, 15O–15V).

In all of the gladii substrates (Fig. 14), including the mantle and ink sac remains (Fig. 15), apatite minerals are covered by carbonaceous material and encrusted by accessory minerals, including calcite, barite, sphalerite,

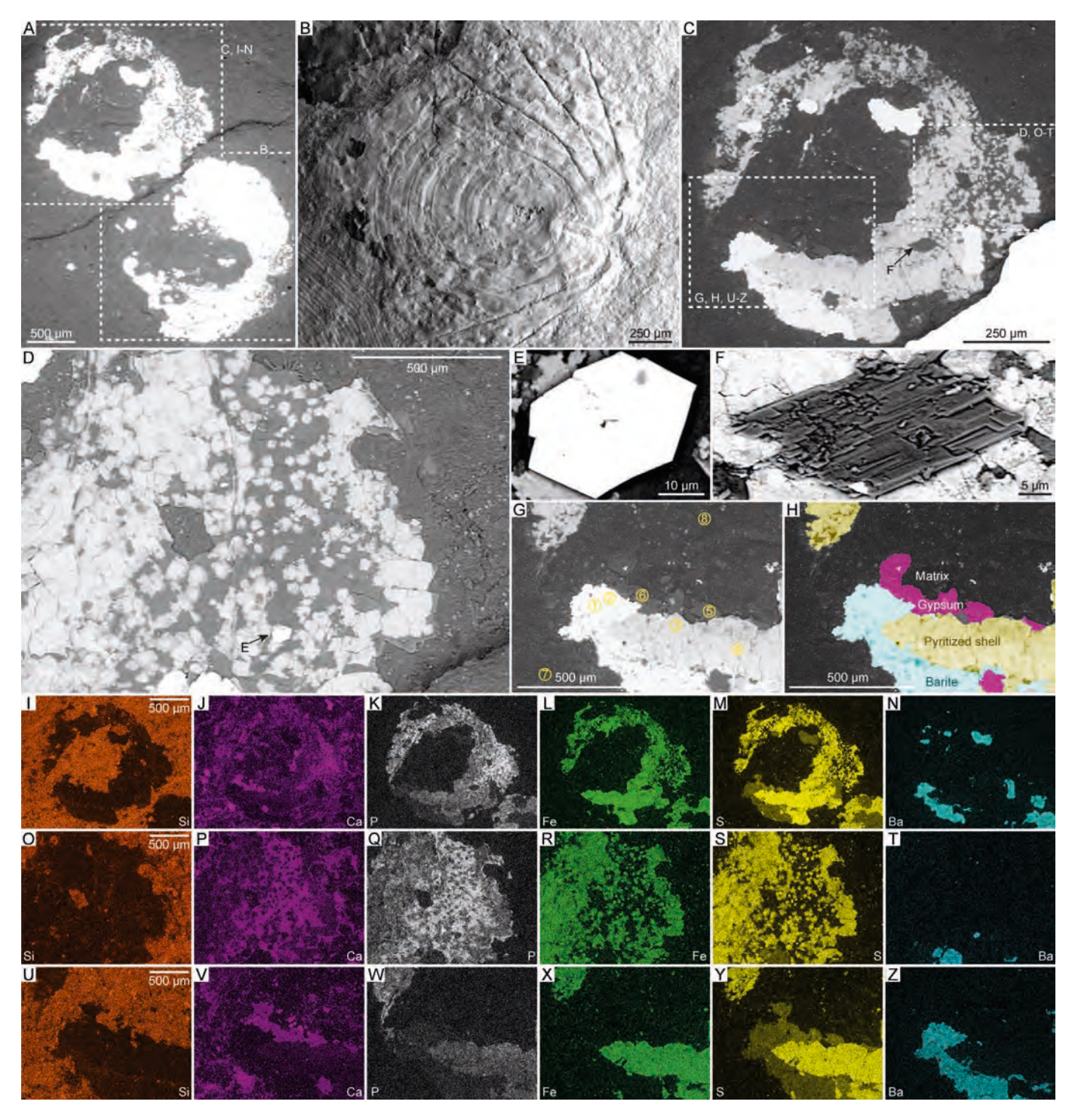


Fig. 5.—Pyritized fossils of the linguliformean (inarticulate) brachiopod *Discinisca* (TMP2015.050.0254; Toarcian, 14.6 m in section, Poker Chip Shale, East Tributary). A–H) BSE images. All of these images were acquired with the compositional imaging mode, except for B, which was produced using the topographic imaging mode: A) Overview of fossils. B) Magnified image of box in A, showing ridges on the surface of one shell. C) Magnified image of box in A, showing the various minerals found in one of the fossils. D) Magnified image of box in C, showing contrast between phosphatic and pyritic shell material. E) Magnified image of area indicated by arrow in D, corresponding to a euhedral barite crystal. F) Magnified image of area indicated by arrow in C, indicating a layered aggregate of sheet-like gypsum. G) Magnified image of box in C, showing gypsum and barite surrounding pyritized shell. Numbered circles enclose points, which were analyzed with EDS to collect semi-quantitative elemental concentration data (Fig. 6). H) Illustration of minerals and materials in G. I–Z) EDS elemental maps: I–N) View in C. O–T) View in D. U–Z) View in G and H.

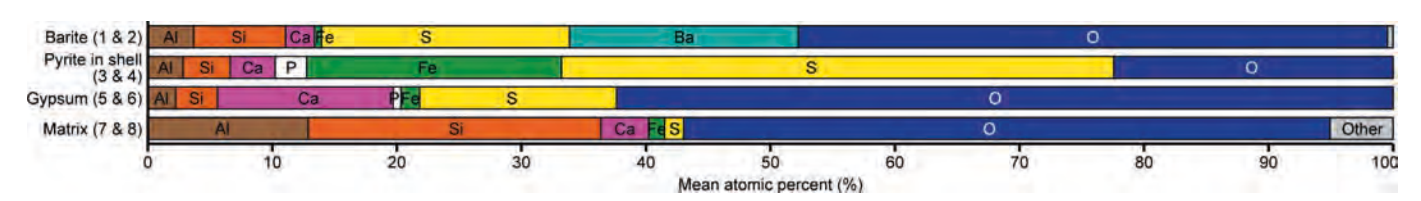


Fig. 6.—Semi-quantitative elemental concentration data from pyritized *Discinisca* fossils (TMP2015.050.0254; Toarcian, 14.6 m in section, Poker Chip Shale, East Tributary). Numbers in parentheses correspond to points in the BSE images of Figure 5G. Bar plot illustrates the data, which are reported as mean (normalized) atomic percentages.

pyrite, and aluminosilicate clays (Figs. 14E–14Z, 16, 17). The calcite and barite occur as large euhedral crystals on the exterior surfaces of the substrates, and the aluminosilicate clays make up thin veneers on the fossils, which are evident in elemental maps as areas of high Al, Fe, Mg, and O (but low K and Si) concentration relative to the surrounding rock matrix (Figs. 16, 17). Pyrite and sphalerite occur as cements in the rock surrounding the fossils, and in some cases, as thin crusts on the surfaces of the phosphatic material (Fig. 15F, 15O–15V, 16B, 16O–16Z, 17). The elemental maps show that, in addition to high concentrations of Zn and Fe, the sphalerite also includes a high concentration of Na (Fig. 16).

DISCUSSION

Fossil Mineralization

The Red Deer and Poker Chip Shale members of the Fernie Formation at Ya Ha Tinda Ranch contain fossils of various types of organisms and tissues. Ammonites, belemnites, bivalves, crinoids, rhynchonellid brachiopods, and rare gastropods left behind fossils of their calcium carbonate shells (Table 1; Figs. 3, 4, 14). Vampyropod coleoids left behind fossils of their gladii, ink sacs, and mantle tissues (Marroquín et al. 2018), which in life, were likely comprised of biopolymers (e.g., chitin and melanin)

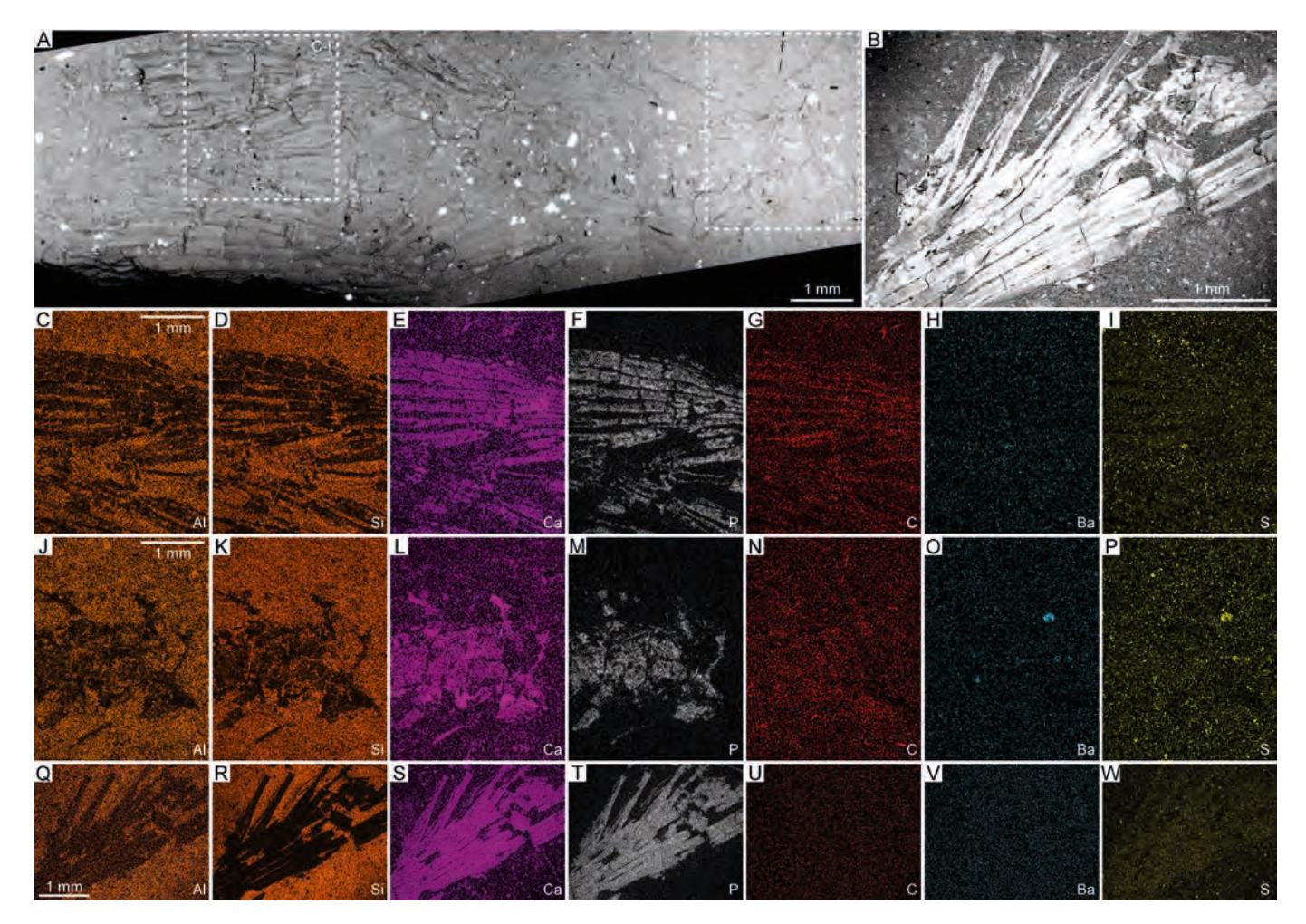


Fig. 7.—Fish vertebrae, ribs, and fins. **A**, **B**) BSE images acquired with the compositional imaging mode: **A**) Composite image of the fossil in Figure 3R (TMP2015.0 51.0118; Toarcian, 1.2–1.6 m in section, Poker Chip Shale Member, Scalp Creek). **B**) Magnified image of the box in Figure 3S (TMP2015.050.0065; Pliensbachian, Red Deer Member, East Tributary). **C**–**W**) EDS elemental maps: **C**–**I**) Box in A (tail fin). **J**–**P**) Box in A (vertebrae and ribs). **Q**–**W**) View in B (fin).

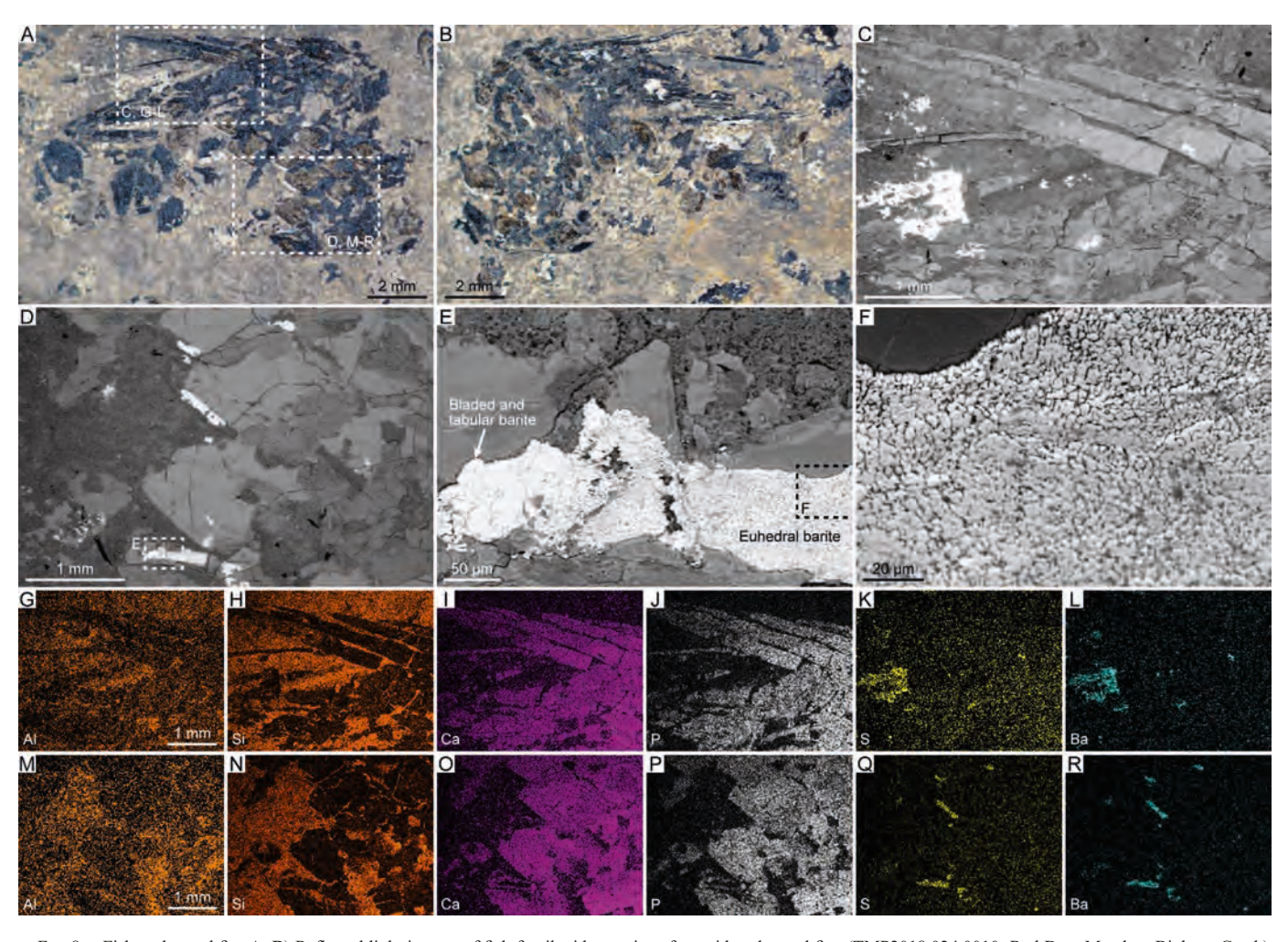


Fig. 8.—Fish scales and fin. **A**, **B**) Reflected light images of fish fossil with remains of ganoid scales and fins (TMP2018.024.0010; Red Deer Member, Bighorn Creek), part and counterpart, respectively. **C**—**F**) BSE images acquired with the compositional imaging mode: **C**) Magnified image of box in A, showing fin encrusted by barite. **D**) Magnified image of box in A, showing ganoid scales. **E**) Magnified image of box in D, showing phosphatic ganoid scales encrusted by bladed, tabular, and euhedral barite, as identified by the arrows and labels. **F**) Magnified image of box in E, showing euhedral barite crystals on the surface of a scale. **G**—**R**) EDS elemental maps: **G**—**L**) View in C. **M**—**R**) View in D.

resistant to degradation (Hunt and Nixon 1981; Donovan and Toll 1988; Doguzhaeva and Mutvei 2003; Glass et al. 2012). All of the other fossils from the units represent substrates that originally contained biominerals made of calcium phosphate (i.e., minerals of the apatite group). Fish skeletal elements are generally composed of collagen and bioapatite, a unique form of carbonate hydroxyapatite characterized by small (nm-sized) crystals, low OH content, and poor crystallinity (Onozato and Watabe 1979; Ikoma et al. 2003; Szpak 2011; Combes et al. 2016). Linguliformean brachiopod shells and crustacean exoskeletons, in contrast, are comprised of mineralized layers. A linguliformean shell typically consists of three layers: (1) an outermost periostracum made of chitin; (2) a thin primary layer of stratiform laminae composed of glycosaminoglycan polysaccharides and carbonate fluorapatite; and (3) an innermost secondary layer of lamellar material made up of glycosaminoglycan polysaccharides, chitin, apatitic granules, and in some cases, collagen (Watabe and Pan 1984; Williams and Holmer 1992; Williams et al. 1992; Cusack and Williams 1996; Cusack et al. 1999; Balthasar 2007; Zabini et al. 2012). Likewise, the carapace of a decapod crustacean generally consists of a waxy (outer) epicuticle that serves as a barrier to diffusion and a chitinous (inner) procuticle that provides mechanical support. The procuticle, in turn, is comprised of a tough exocuticle and flexible endocuticle, which in some cases, are separated by a mesocuticle (Kunkel et al. 2012; Kunkel 2013). Although decapod exoskeletons are not heavily mineralized, these layers of the procuticle sometimes contain biominerals (calcite, amorphous calcium carbonate, and carbonate apatite) that add rigidity (Kunkel et al. 2012; Kunkel 2013). The fossils in the Ya Ha Tinda Lagerstätte, ergo, represent skeletal elements and relatively recalcitrant tissues. Labile muscles, organs, and integuments are rare or absent.

With the exception of the originally aragonitic and calcitic shells, which are preserved as calcified fossils and non-mineralized impressions (Figs. 3A–3I, 3K, 3L, 4), all of the specimens collected from Ya Ha Tinda are composed, at least in part, of calcium phosphate minerals of the apatite group (e.g., hydroxyapatite and fluorapatite). Although fossils containing these minerals typically fluoresce under UV light, none of the specimens exhibit fluorescence outside areas where they are encrusted or crosscut by calcite (Martindale et al. 2017). The high concentration of organic matter in the fossils, particularly the presence of carbonaceous layers, may limit the perception of fluorescence. Even so, combined BSE and EDS demonstrates that apatite minerals are present in a variety of fossilized substrates in the Konservat-Lagerstätte, including organophosphatic shells (Fig. 5), bones (Figs. 7, 9, 10), fins (Figs. 7–9), scales (Fig. 8), decapod cuticles (Figs. 11–13), and coleoid gladii (Figs. 14–17), mantle (Figs. 15,

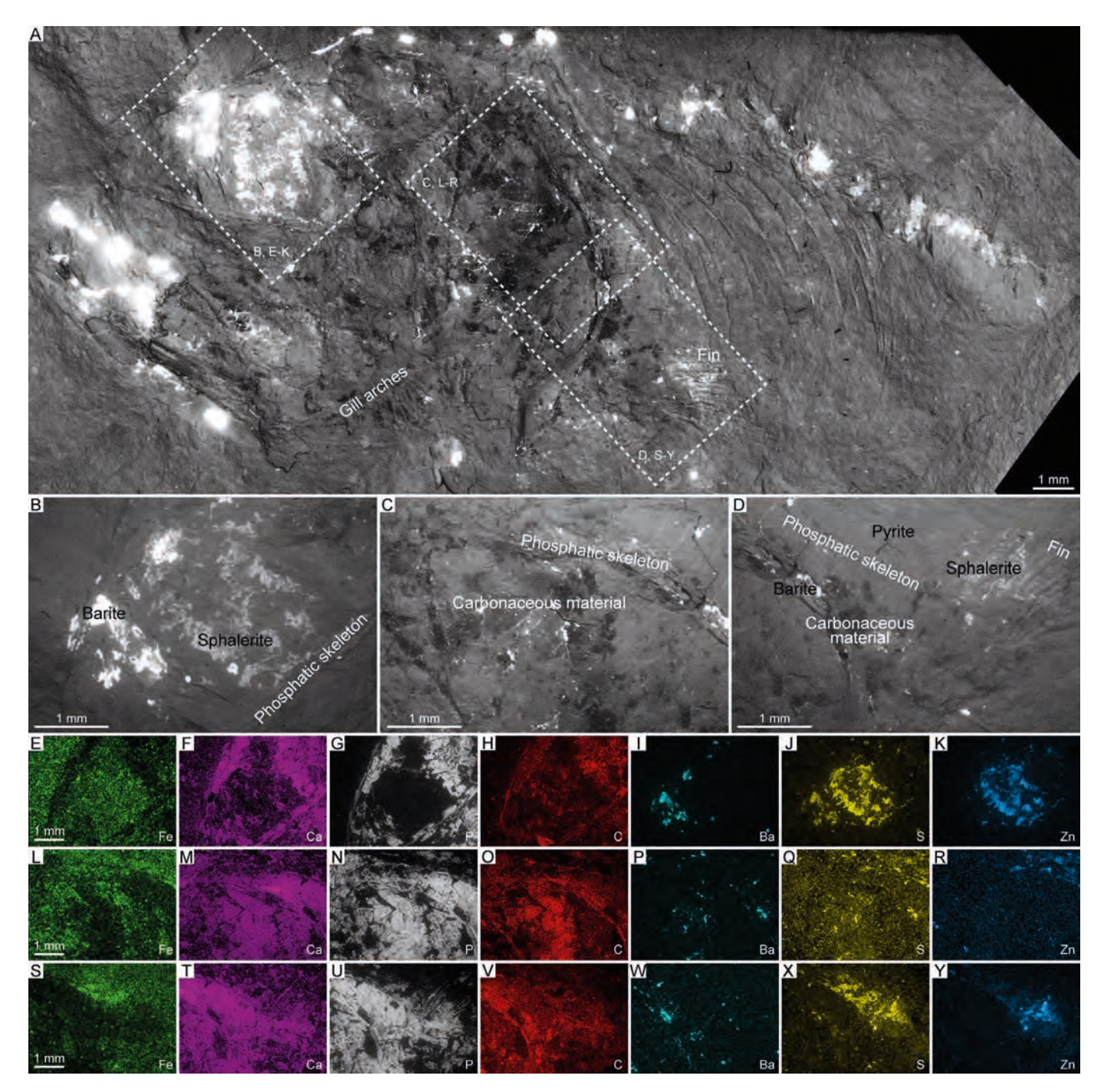


Fig. 9.—Articulated fish with fins and gill arches (counterpart, TMP2014.021.0043b; Toarcian, 16 m in section, Poker Chip Shale Member, East Tributary). Fossil is counterpart of specimen illustrated in Figure 3T. A–D) BSE-SEM images acquired with compositional imaging mode: A) Mosaic image. B) Magnified image of box in A, showing barite and sphalerite associated with phosphatic skull material. C) Magnified image of box in A, showing carbonaceous material covering phosphatic skeleton (e.g., rib remains). D) Magnified image of box in A, showing the barite, sphalerite, and pyrite associated with carbonaceous and phosphatic skeletal material near the fin of the fish. E–Y) EDS elemental maps: E–K) View in B. L–R) View in C. S–Y) View in D.

16), and ink sac remains (Figs. 15, 17). Many of these substrates originally contained apatite minerals in one form or another. Nonetheless, phosphatic coleoid gladii indicate that secondary phosphate mineralization of the substrates—a process called phosphatization—played a constructive role in the preservation of some or all of the fossils.

Phosphatization represents one of a number of taphonomic processes that can contribute to fossil preservation (Allison 1988b; Briggs et al.

1993; Briggs and Wilby 1996; Briggs 2003; Butterfield 2003; Xiao and Schiffbauer 2009; Schiffbauer et al. 2014a; Muscente et al. 2015a, 2017b). The process receives much attention for its role in the preservation of labile tissues and in some cases subcellular details, as it results in the replication of organic templates with nanometer- and micrometer-sized apatite crystals (Allison 1988a; Martill 1988; Wilby 1993; Wilby and Whyte 1995; Xiao and Knoll 1999; Waloszek 2003; Xiao and Schiffbauer 2009; Schiffbauer

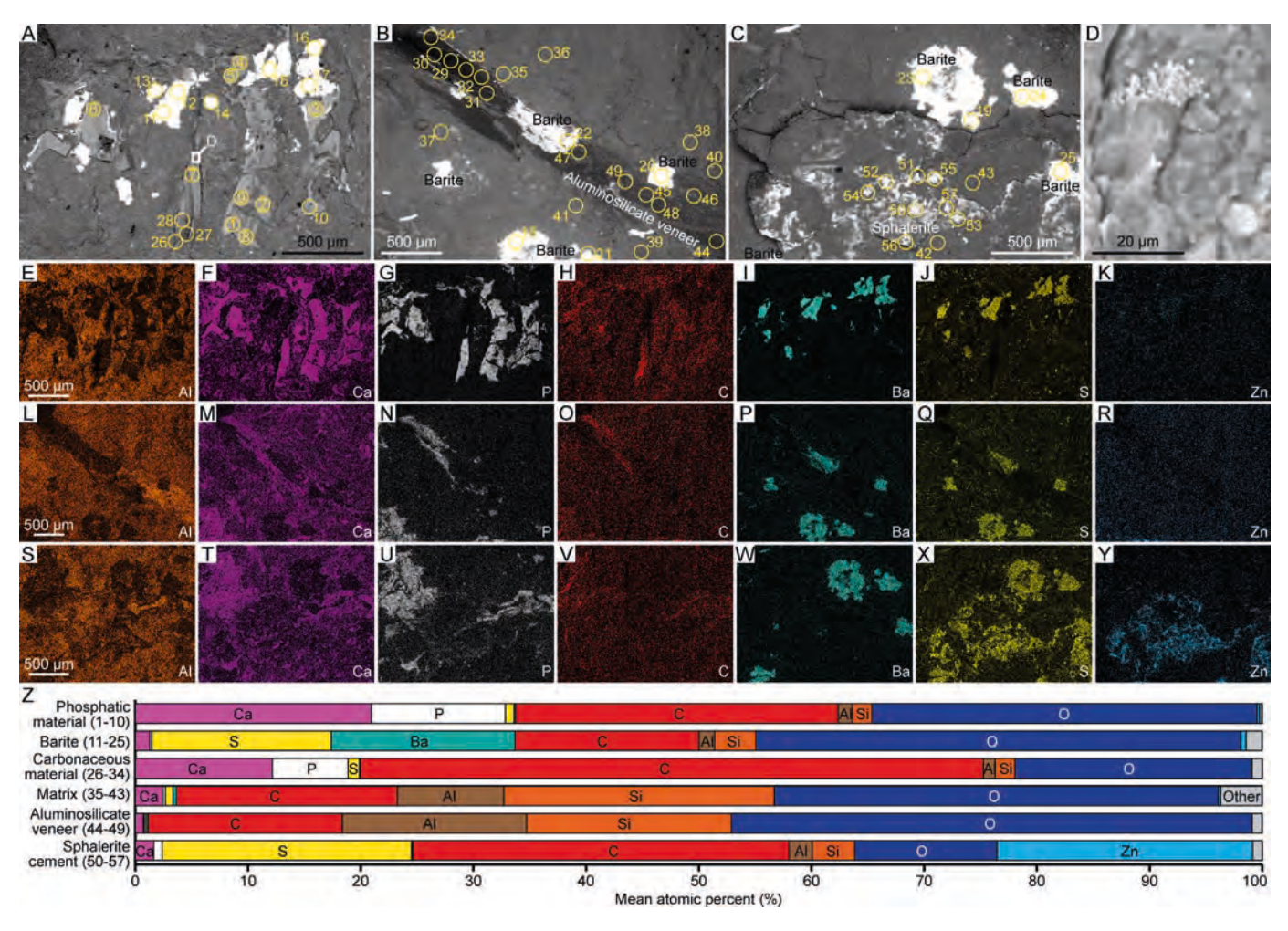


Fig. 10.—Minerals found in an articulated fish fossil (part, TMP2014.021.0043a; Toarcian, 16 m in section, Poker Chip Shale Member, East Tributary). A–D) BSE images acquired with the compositional imaging mode. Numbered circles enclose points, which were analyzed with EDS to collect semi-quantitative elemental concentration data: A) Magnified image of box in Figure 3T, showing that the vertebrae and ribs are preserved as phosphatic and carbonaceous materials encrusted by barite. B) Magnified image of box in Figure 3T, showing that the skull is preserved, in part, as carbonaceous material with an aluminosilicate veneer and barite crust. C) Magnified image of box in Figure 3T, showing barite and sphalerite cements in matrix around fossil. D) Magnified image of box in A, showing pyrite framboids in matrix around the vertebrae and ribs. E–Y) EDS elemental maps: E–K) View in A. L–R) View in B. S–Y) View in C. Z) Bar plot illustrating the elemental concentration data, which are reported as mean (normalized) atomic percentages. Numbers in parentheses correspond to points in the BSE images.

et al. 2012; Hawkins et al. 2018). In the case of the Ya Ha Tinda fossils, the precipitation and growth of apatite provides the best explanation for the preservation of non-biomineralized coleoid tissues and the weaklybiomineralized crustacean carapaces. Secondary phosphatization can also enhance the preservation potential of phosphatic, calcitic, and aragonitic skeletal elements (Porter 2004; Creveling et al. 2014b). In addition, because environments conducive to phosphatization are characterized by high concentrations of dissolved phosphate (Creveling et al. 2014a; Muscente et al. 2015a), they are also generally favorable for the preservation of phosphatic skeletons, as their conditions limit the potential for fossil dissolution. Thus, phosphatization may have directly contributed to the preservation of linguliformean brachiopods and fish skeletons at Ya Ha Tinda, or those fossils simply represent another consequence of an environment conducive to phosphatization. Future work on the ultrastructure and recrystallization of the brachiopod and fish fossils may shed light on the role that secondary phosphate mineralization may have played in their preservation.

A number of specimens from Ya Ha Tinda contain carbonaceous material in addition to apatite minerals. The material is visible in BSE images as a dark (low Z) compound (Figs. 9A, 9C, 9D, 10B, 11C, 12B-12D, 13F, 13G, 14F, 14H, 15C, 15E, 15F, 16A, 16B, 17A), and is similar in appearance to organic matter described from other exceptionally preserved fossils (Orr et al. 2002, 2009; Muscente et al. 2015b, 2017a; Muscente and Xiao 2015a, 2015b). The fossils at Ya Ha Tinda exhibit topographic relief on the order of tens to hundreds of micrometers, as demonstrated by reflected light images acquired with directional illumination (Fig. 13A-13C), BSE images produced with the topographic imaging mode (Fig. 5B), and SE images with topographic contrast (Figs. 12A, 14C, 15D). Hence, none of the fossils in the Konservat-Lagerstätte qualify as 'carbonaceous compressions', which in general, are thin (<1 µm thick) layers of flattened carbonaceous material (Orr et al. 2002; Martí Mus 2014; Muscente and Xiao 2015b). Evidently, the fossils did not experience the same degree of burial compaction as carbonaceous compressions (Rex and Chaloner 1983; Rex 1986; Martí Mus 2014), suggesting that phosphatization occurred prior to compaction and contributed to the retention of topographic relief. Although some of the fossilized remains consist of carbonaceous material in places (Figs. 10B, 11C, 13F, 13G), the bulk of these remains are comprised of apatite minerals (Figs. 10A, 10E-10R, 11C, 11E-11K, 13D-

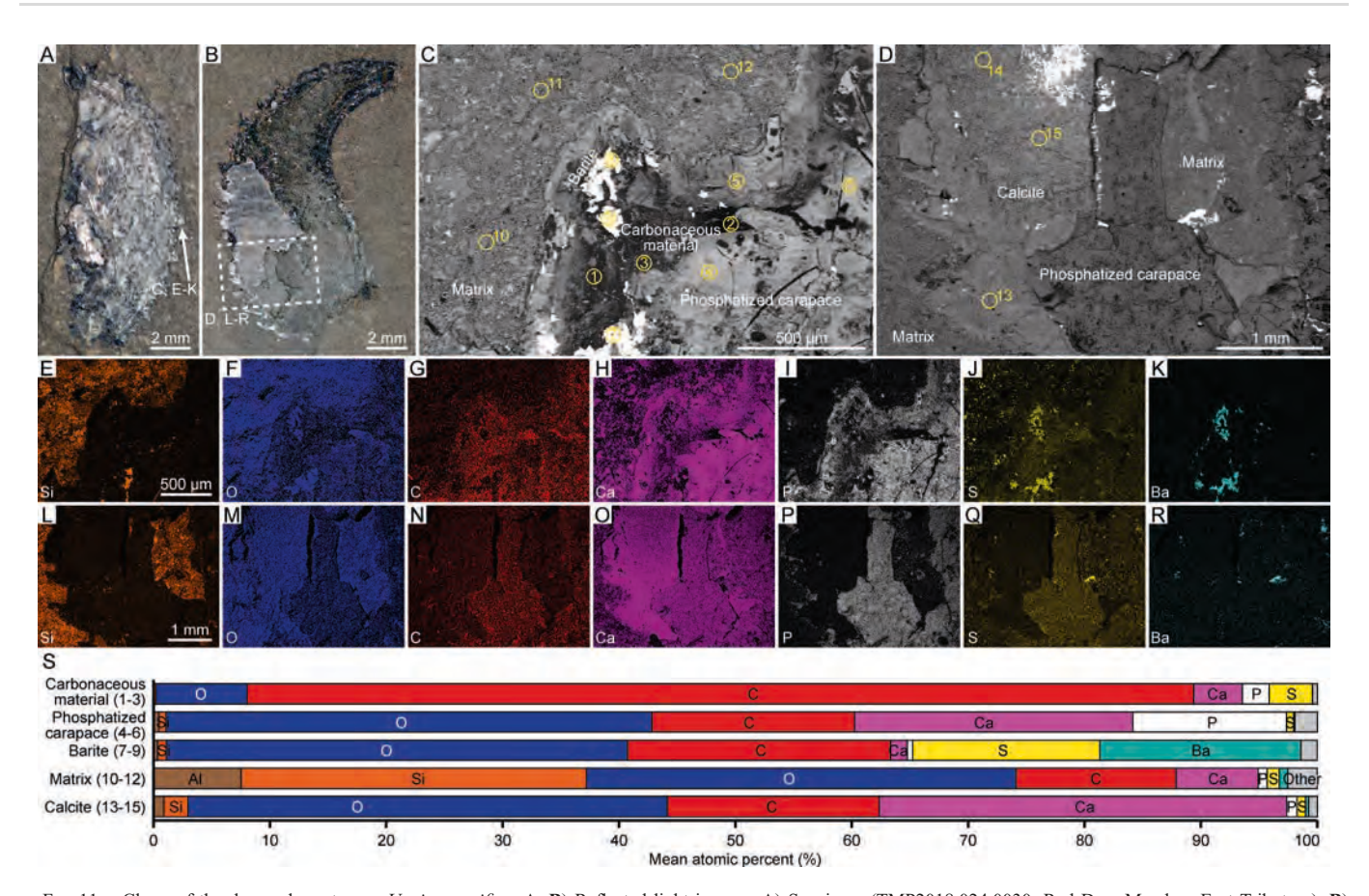


Fig. 11.—Claws of the decapod crustacean *Uncina pacifica*. **A**, **B**) Reflected light images: **A**) Specimen (TMP2018.024.0030; Red Deer Member, East Tributary). **B**) Specimen (TMP2018.024.0037; Red Deer Member, East Tributary). **C**, **D**) BSE images acquired with the compositional imaging mode. Numbered circles enclose points, which were analyzed with EDS to collect semi-quantitative elemental concentration data: **C**) Magnified image of area indicated by arrow in A, showing the phosphatized carapace and carbonaceous material of the fossil along with encrusting barite. **D**) Magnified image of box in B, showing the phosphatized carapace of the fossil and encrusting calcite. **E**–**R**) EDS elemental maps: **E**–**K**) View in C. **L**–**R**) View in D. **S**) Bar plot illustrating the elemental concentration data, which are reported as mean (normalized) atomic percentages. Numbers in parentheses correspond to points in the BSE images.

13U), which are likely more resistant to compaction than non-biomineralized tissues (Briggs 2003).

The fossils are associated with a number of minerals besides those of the apatite group. These minerals include pyrite, sphalerite, barite, calcite, gypsum, and aluminosilicate clays. Although all of these minerals occur throughout the strata, BSE imaging suggests that they are most common and concentrated near fossils. We found barite, for example, in association with shelly fossil (Fig. 5), fish (Figs. 8-10), crustacean (Figs. 11-13), and coleoid specimens (Figs. 14-16). Notwithstanding, none of the auxiliary minerals described here occupy spaces representing skeletal or exceptionally preserved tissues, except for pyrite, which occurs in the fossils of some brachiopods (Fig. 5), bivalves, and ammonites (Martindale et al. 2017). These fossils represent consequences of pyritization, or the process of pyrite precipitation and growth on biologic templates (Briggs et al. 1996; Schiffbauer et al. 2014b; Guan et al. 2016), although pyritized fossils are uncommon in the Red Deer and Poker Chip Shale members. Unlike the Highwood Member, which contains many pyrite-rich layers, most of the pyrite in the Lagerstätte occurs as framboids and euhedral crystals (Figs. 9D, 10D, 16B), and very rarely, as nodules in the rock matrix. Barite and sphalerite are also present as cements in the matrix (Figs. 10C, 16). In other places, barite encrusts the phosphatic and carbonaceous materials that make up the fossils (Figs. 5G, 5H, 8D-8F, 9B, 9E-9K, 10A, 10B, 10E-10R, 11C, 11E-11K, 14E, 14G, 14H, 14O-14Z, 16). Likewise, calcite occurs in crusts around

phosphatized carapaces (Figs. 11D, 12C–12R, 13B–13D, 13H–13N) and coleoid remains (Figs. 14G, 14H, 14O–14Z, 16A, 16C–16N, 17); gypsum surrounds some pyritized linguliformean brachiopod shells (Fig. 5F–5H, 5U–5Z); and aluminosilicate clays make up thin (nm thick) veneers located between fossil substrates and surrounding rock (Figs. 10B, 10L–10R, 16A, 16C–16N). Notably, we found calcite crusts in decapod crustaceans with carbonaceous and phosphatic layers (Fig. 12, 13). These layers may represent the epicuticle and procuticle, respectively. Regardless, neither the calcite crusts nor the carbonaceous layers in these specimens show evidence of ornamentation (i.e., low-relief bumps in Fig. 13B, 13C); the morphological ornamentation is restricted to the phosphatized carapace. Thus, the calcite does not conserve the ultrastructural characters of the carapace. These various observations suggest that the auxiliary minerals formed after phosphatization, and their pathways of formation were not essential to fossil preservation.

Altogether, our results support limited data that were previously reported suggesting that the fossils at Ya Ha Tinda consist of organic matter, apatite, and clay minerals (Martindale et al. 2017). Our work also confirms that, although the exceptionally preserved fossils experienced significant amounts of burial compaction, they are not 'two-dimensional compressions', as previously described (Martindale et al. 2017), and retain topographic relief at a sub-millimeter scale (Fig. 5B, 11D, 13B, 14B, 15D). This relief corroborates the hypothesis that the preservational pathway of the Konservat-Lagerstätte involved phosphatization in addition to skeletal

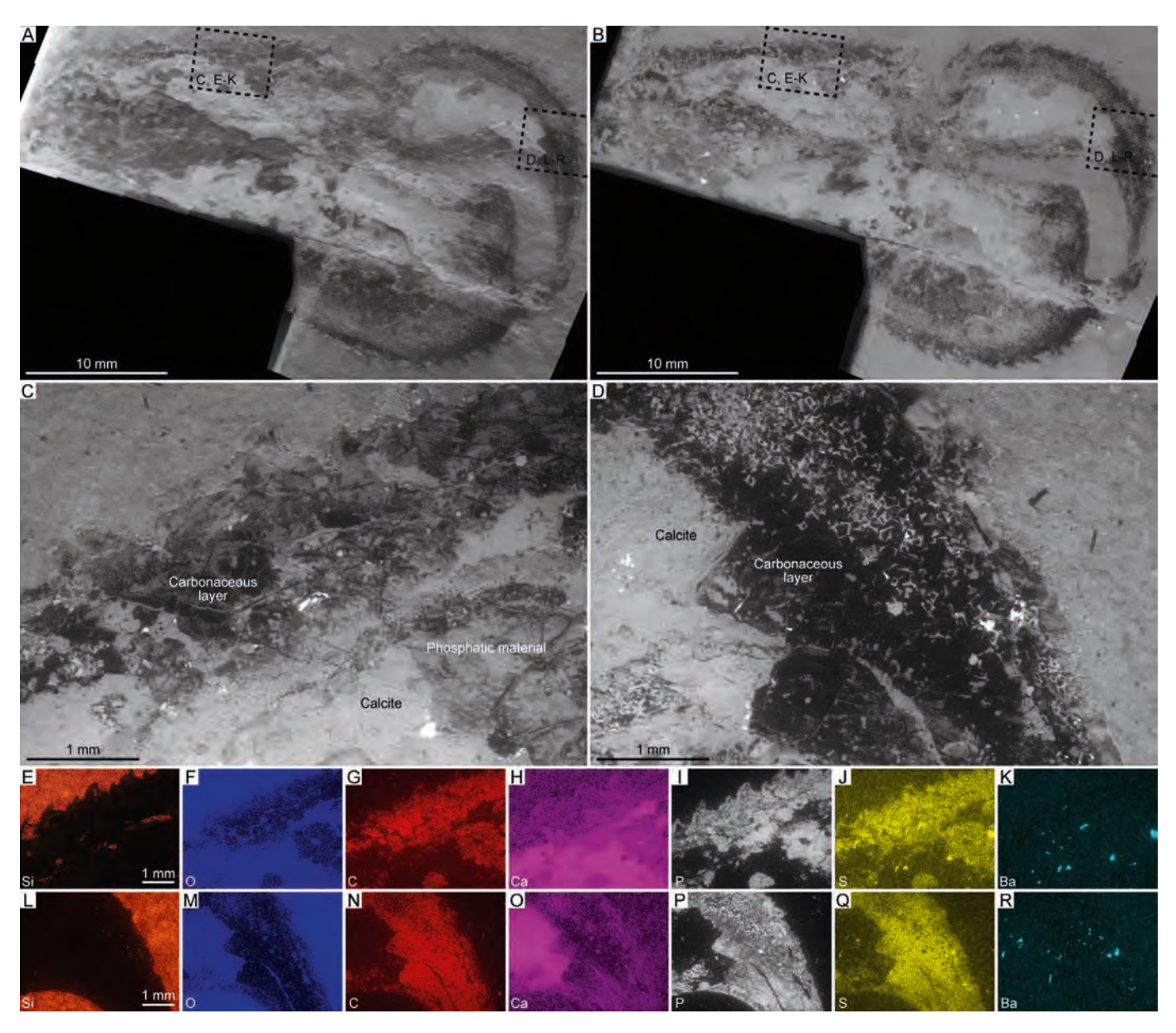
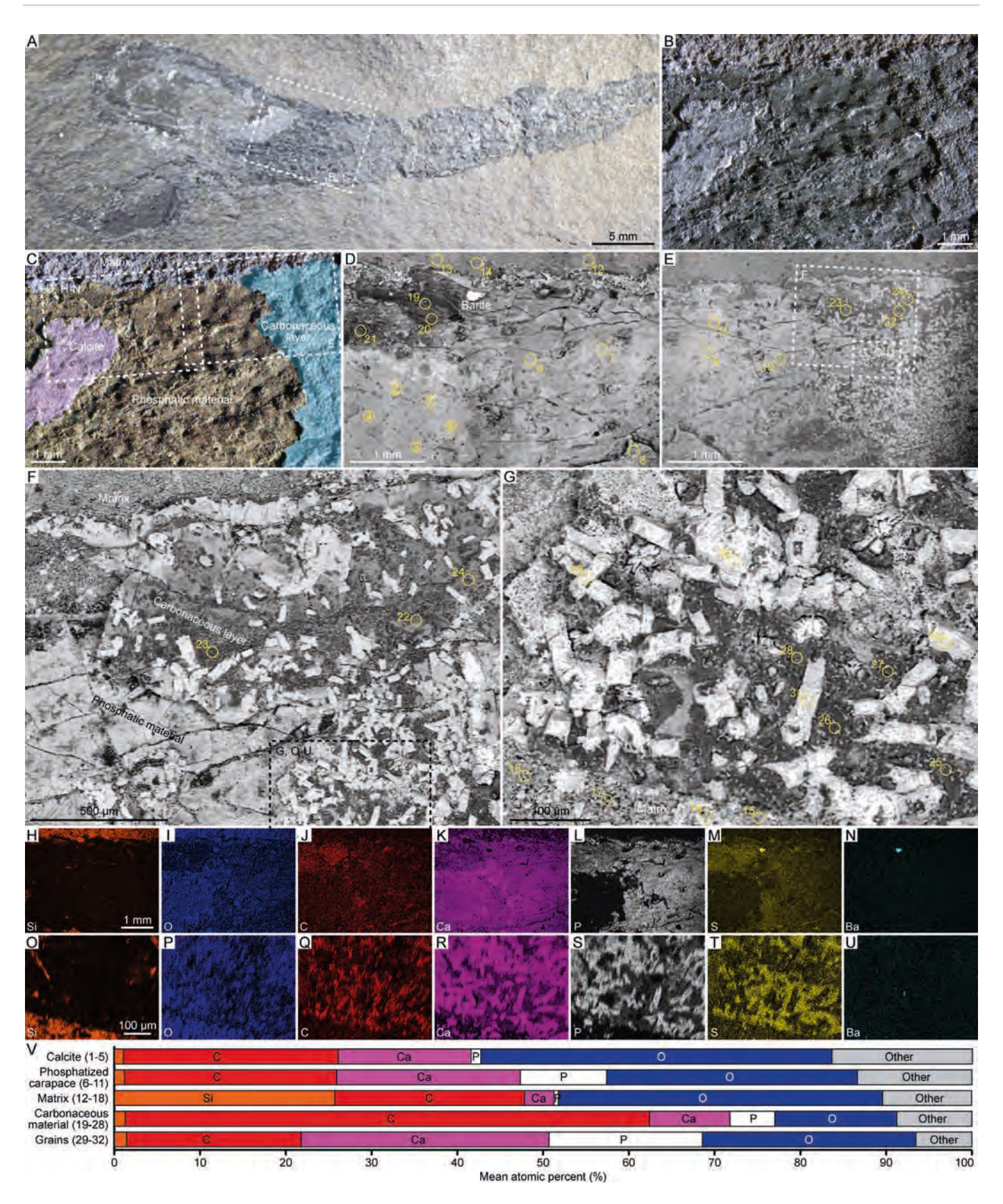


Fig. 12.—Claw on the holotype specimen of the decapod crustacean *Uncina pacifica* (TMP2002.043.0005; *margaritatus* Zone, Pliensbachian, Red Deer Member, East Tributary). **A–D**) SEM images: **A**) Mosaic SE image. **B**, **C**) BSE images acquired with compositional imaging mode: **B**) Mosaic BSE image. **C**) Magnified image of boxes in **A** and **B**, showing the phosphatized carapace and carbonaceous material of the fossil along with encrusting calcite. **D**) Magnified image of boxes in A and B, showing the same materials. **E–R**) EDS elemental maps: **E–K**) View in C. **L–R**) View in D.

and organic matter preservation (Martindale et al. 2017). Like previous studies, we found little evidence of fossil pyritization (Martindale et al. 2017). Accordingly, paleoenvironmental reconstructions and taphonomic models for the Ya Ha Tinda deposit must account for the presence of

phosphatized fossils and articulated skeletons in addition to the paucity of pyritized fossils, which are common in coeval black shales (e.g., the Jet Rock Formation) and marine Lagerstätten, like the Posidonia Shale (Hudson 1982; Littke et al. 1991; Montero-Serrano et al. 2015).

Fig. 13.—Layers of lobster carapace fossil (*Uncina pacifica*). A–C) Reflected light images: A) Overview of specimen (TMP2002.043.0004; *margaritatus* Zone, Pliensbachian, Red Deer Member, East Tributary). B) Magnified image of box in A, showing outer (non-ornamented) carbonaceous and inner (ornamented) phosphatic layers of the carapace along with encrusting calcite. The inner layer of phosphatic material is ornamented with low-relief bumps. Image was acquired under directional illumination with the source of light located right of the field of view. C) Illustration of layers in B. D–G) BSE images acquired with the compositional imaging mode. Numbered circles enclose points, which were analyzed with EDS to collect semi-quantitative elemental concentration data: D) Magnified image of box in C, showing phosphatic and carbonaceous materials in the carapace along with encrusting calcite and barite. E) Magnified image of box in C, showing the non-ornamented (carbonaceous) and ornamented (phosphatic material) layers of the carapace. F) Magnified image of box in E, showing the carbonaceous layer on top of the phosphatic material. G) Magnified image of the boxes in E and F, showing phosphatic granules in the carbonaceous layer. H–U) EDS elemental maps: H–N) View in D. O–U) View in G. V) Bar plot illustrating the elemental concentration data, which are reported as mean (normalized) atomic percentages. Numbers in parentheses correspond to points in the BSE images.



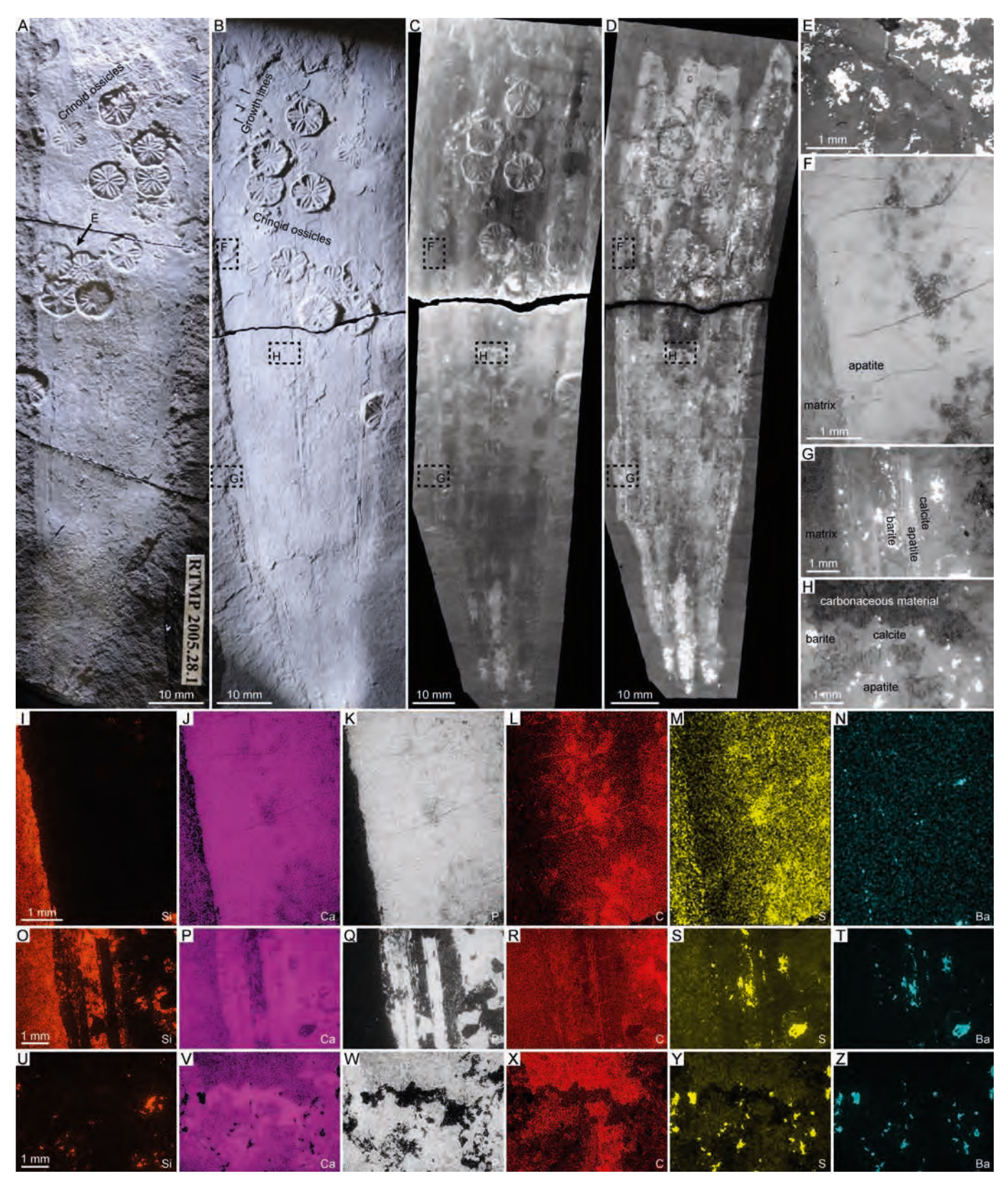


Fig. 14.—Phosphatized gladius of the coleoid *Paraplesioteuthis* cf. *sagittata* (TMP2005.028.0001; *margaritatus* Zone, Pliensbachian, Red Deer Member, East Tributary). The gladius contains growth lines and was preserved with, and most likely deposited upon, the disarticulated ossicles of the crinoid *Seriocrinus subangularis* (Marroquín et al. 2018). **A, B)** Reflected light images of the fossil after coating with ammonium chloride salt sublimate: **A)** Part (TMP2005.028.0001a). **B)** Counterpart (TMP2005.028.0001b). **C–H)** SEM images of fossil: **C)** Mosaic SE image of counterpart. **D–H)** BSE images acquired with compositional imaging mode: **D)** Mosaic BSE image of counterpart. **E)** Magnified image of the edge of a crinoid ossicle, as indicated by arrow in A. **F)** Magnified image of boxes in B–D, showing edge of phosphatized gladius with carbonaceous material and surrounding matrix. **G)** Magnified image of boxes in B–D, showing barite, calcite, and matrix material near edge of phosphatized gladius. **H)** Magnified image of boxes in B–D, showing barite, calcite, and carbonaceous material on the phosphatized gladius. **I–Z)** EDS elemental maps: **I–N)** View in F. **O–T)** View in G. **U–Z)** View in H.

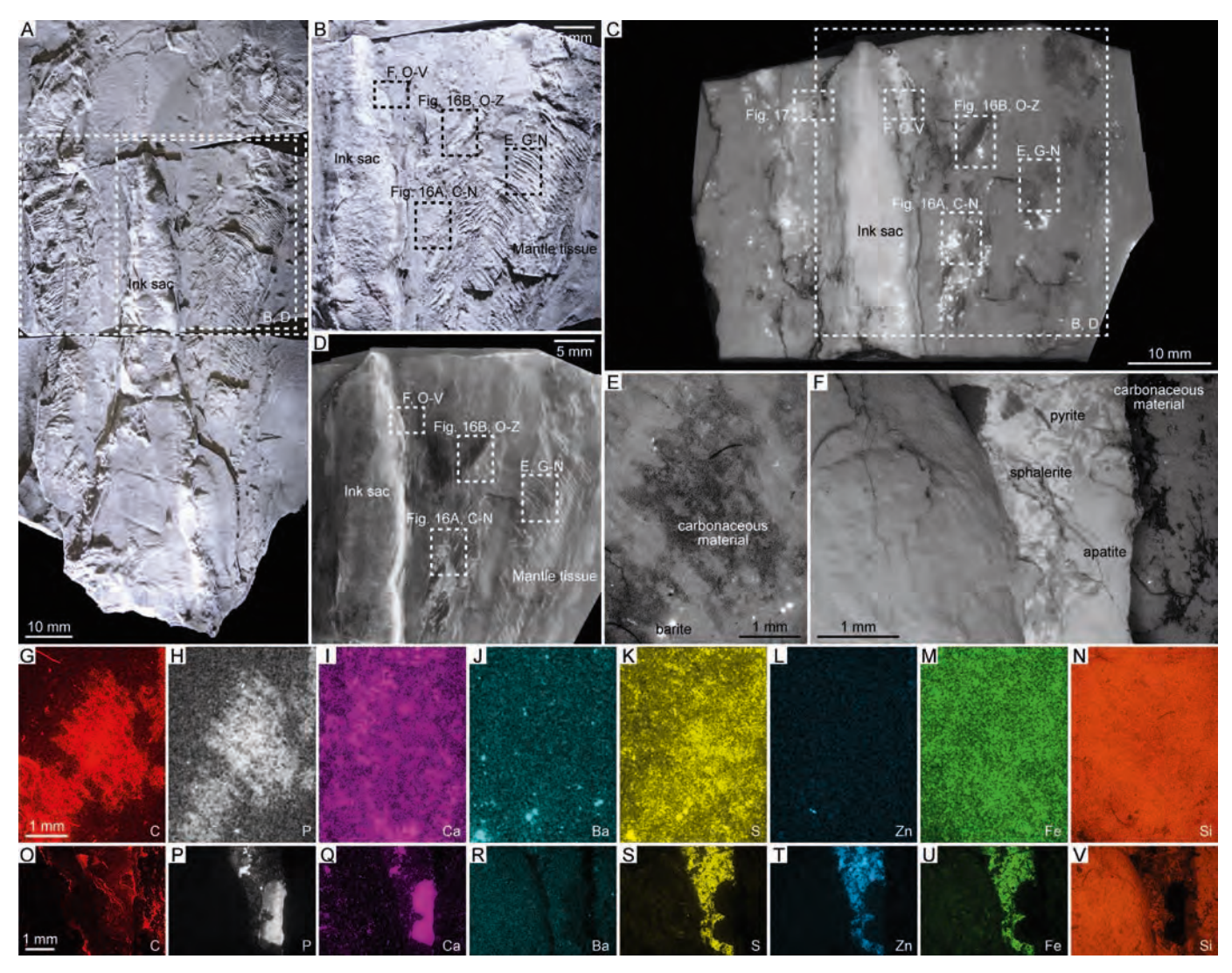
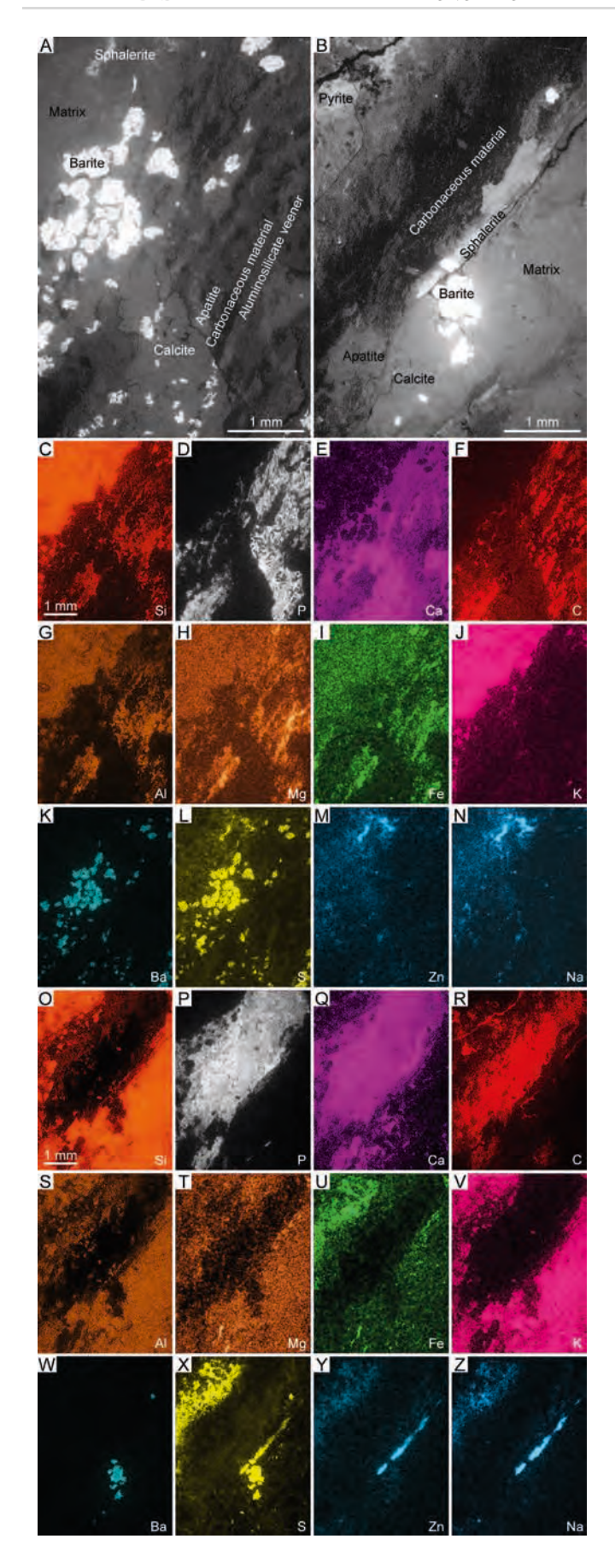


Fig. 15.—Coleoid gladius (Suborder Loligosepiina) with mantle and ink sac remains (TMP2013.036.0008; *planulata* Zone, Toarcian, 16.8 m in section, Poker Chip Shale Member, East Tributary). **A, B)** Reflected light images of the fossil after coating with ammonium chloride salt sublimate: **A)** Part of specimen (TMP2013.036.0008a). **B)** Magnified image of small box in **A**, showing mantle material and ink sac. **C**–**F)** SEM images (BSE images were acquired in the compositional imaging mode): **C)** Mosaic BSE image of the large box in A. **D)** Mosaic SE image of B and boxes in A and C. **E)** A magnified BSE image of the boxes in B–D, showing carbonaceous material on the surface of the mantle remains. **F)** A magnified BSE image of the boxes in B–D, showing edge of ink sac. **G–V)** EDS elemental maps: **G–N)** View in E. **O–V)** View in F.

Ocean Redox Conditions

Phosphatization generally involves a number of physical and chemical processes, which are sensitive to redox conditions (Schiffbauer et al. 2014a; Muscente et al. 2015a). Anoxic conditions likely prevailed in the depositional environment at Ya Ha Tinda during the late Pliensbachian and early Toarcian for, at least, some periods of time. The anoxia hypothesis originated with the first descriptions of the organic-rich black shales (Stronach 1984), which were interpreted as consequences of high organic matter preservation in fine marine sediments under low oxygen levels (Richards and Redfield 1953). Early work on the paleontology of the Red Deer and Poker Chip Shale members, which revealed abundant pelagic taxa (e.g., ammonites, belemnites, and radiolarians) but few infaunal body or trace fossils, supported the hypothesis and suggested that the seafloor did not typically sustain benthic life (Hall 1987). Discoveries of exceptionally preserved fossils (Hall 1985; Hall and Neuman 1989), particularly those of articulated skeletons, were also interpreted as support for the hypothesis (Hall 1991; Hall et al. 1998; Maxwell and Martindale 2017), as anoxic basins are often invoked as explanations for exceptionally preserved fossils (Seilacher 1982; Seilacher et al. 1985). Finally, geochemical redox proxy data on the iron speciation and thallium isotope profiles of the East Tributary section were published that corroborate the anoxia hypothesis (Fig. 2), suggesting that euxinic bottom water was common in the area from the late Pliensbachian to the early Toarcian (Them et al. 2018). These redox proxy data indicate that bottom water euxinia developed prior to the Toarcian OAE in the late Pliensbachian, suggesting that the site resided within an oxygen minimum zone before the event (Fig. 18A). Problematically, the interval of supposed anoxia contains body and trace fossils of benthic animals at multiple levels (Figs. 2, 3; Martindale and Aberhan 2017), which demonstrate that bottom water euxinia did not persist in the area throughout the Pliensbachian-Toarcian interval. The conflicting data likely indicate that the geochemical signals record long-term trends in ocean chemistry, as opposed to short-term redox fluctuations affecting habitat viability and fossil preservation (Sperling et al. 2016, 2018). The fossil record indicates that oxic and/or dysoxic conditions periodically developed on the seafloor, perhaps for short periods



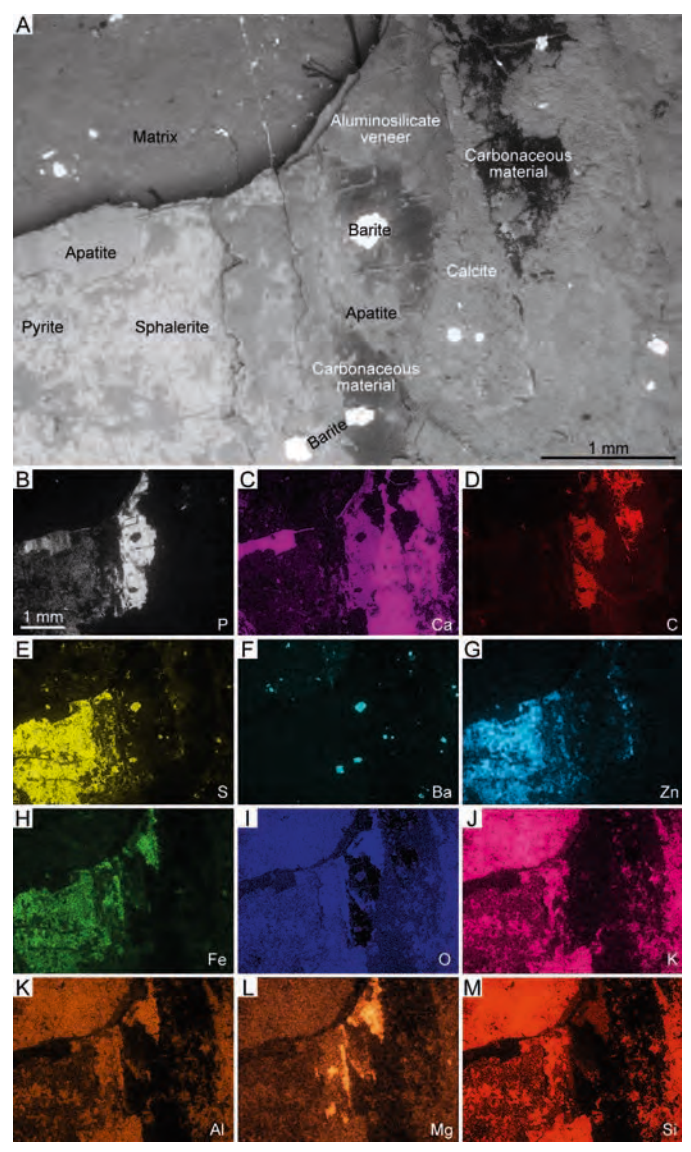


Fig. 17.—Minerals associated with the ink sac remains in the coleoid (Suborder Loligosepiina) gladius (TMP2013.036.0008; *planulata* Zone, Toarcian, 16.8 m in section, Poker Chip Shale Member, East Tributary). A) BSE image, acquired in compositional imaging mode, of the box in Figure 15C, showing phosphatized ink sac encrusted by calcite, pyrite, sphalerite, barite, carbonaceous material, and an aluminosilicate (clay) veneer. **B**–**M**) EDS elemental maps of view in A.

of time, allowing for benthic and infaunal animals to inhabit the environment. Layers with bioturbation and strata containing both large adult and small juvenile benthic taxa (e.g., bivalves and brachiopods) in the upper Pliensbachian, for example, were likely deposited during episodes of

Fig. 16.—Minerals associated with the mantle remains in the coleoid (Suborder Loligosepiina) gladius (TMP2013.036.0008; *planulata* Zone, Toarcian, 16.8 m in section, Poker Chip Shale Member, East Tributary). **A, B)** BSE images acquired in compositional imaging mode: **A)** Magnified image of the boxes in Figure 15 (Fig. 15B, 15C), showing phosphatized mantle encrusted by calcite, sphalerite, barite, carbonaceous material, and an aluminosilicate (clay) veneer. **B)** Magnified image of the boxes in Figure 15 (Fig. 15B, 15C), showing phosphatized mantle surrounded by the sedimentary matrix and encrusted by calcite, sphalerite, barite, pyrite, and carbonaceous material. **C–Z)** EDS elemental maps: **C–N)** View in A. **O–Z)** View in B.

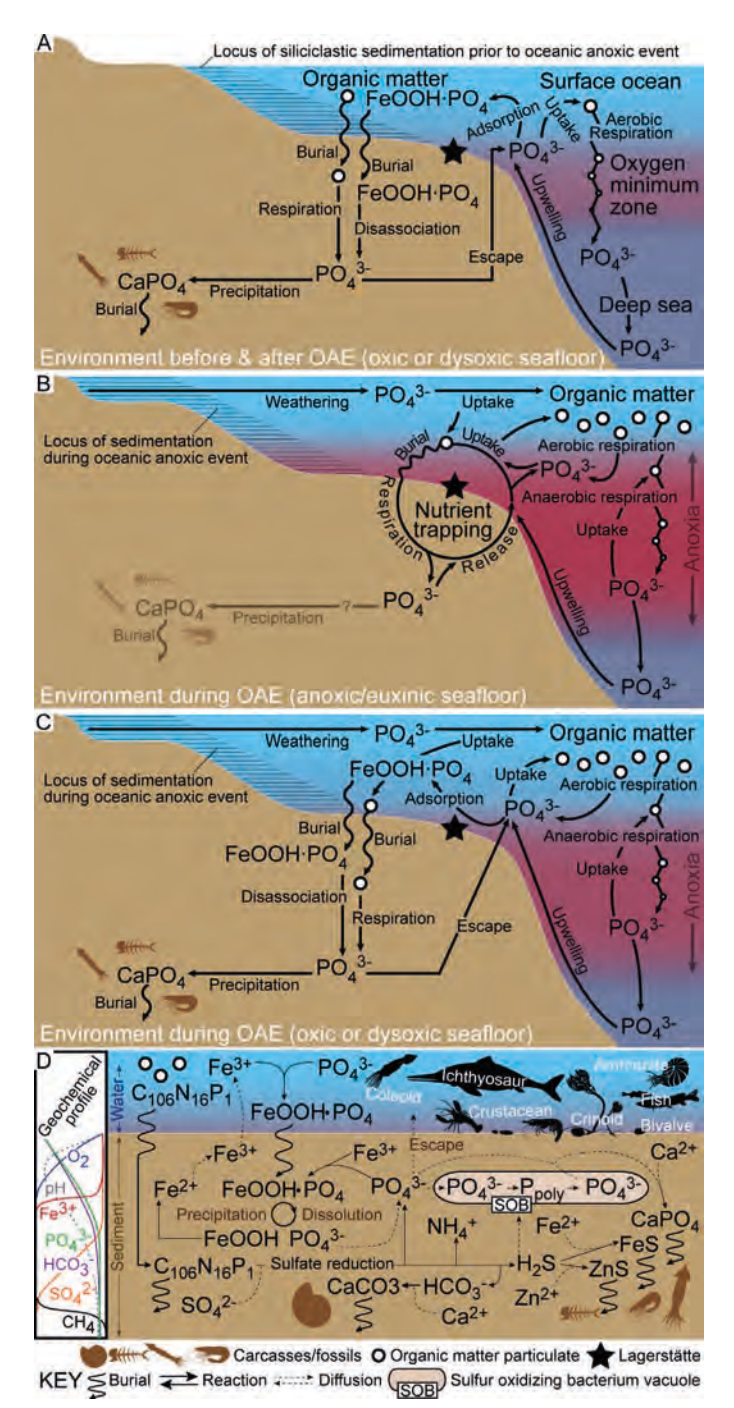


Fig. 18.—Depositional and preservational environment of the Konservat-Lager-stätte in the Jurassic Fernie Formation at Ya Ha Tinda (Alberta, Canada). A–C) Simple shelf-to-basin transects with approximate location of the Lagerstätte, as marked by the star. Arrows illustrate local phosphorus cycle: A) Environment before and after the Oceanic Anoxic Event (OAE). During these times, oxic and/or dysoxic conditions were common on the seafloor; sinking organic matter particulates produced in the surface ocean fueled aerobic respiration, and likely, the development of an oxygen minimum zone; and upwelling of deep sea water provided nutrients to shelf environments, resulting in phosphogenesis (Christie 1989; Poulton and Aitken 1989). B) Euxinic (anoxic) conditions on the seafloor during the OAE. Marine transgression during the OAE likely caused the locus of siliciclastic sedimentation to shift landward; enhanced continental weathering and the delivery of phosphate from land to the ocean; and promoted the release of phosphate from sediment. C) A brief episode of oxic and/or dysoxic conditions on the seafloor during the OAE. These

oxic conditions that persisted for years at a time, possibly between times of dysoxia/anoxia (Martindale and Aberhan 2017). In contrast, non-bioturbated intervals containing exclusively diminutive juvenile and depauperate benthic taxa (e.g., within the Toarcian OAE carbon isotope excursion) were likely deposited under predominantly anoxic/euxinic conditions, when oxia and dysoxia may have developed for only days, weeks, or months at a time (Martindale and Aberhan 2017). Seasonal or annual fluctuations in oxygenation of benthic environments is not uncommon near oxygen minimum zones.

Preservational Environment

The late Pliensbachian-early Toarcian interval at Ya Ha Tinda contains facies of low-energy environments with fluctuating redox conditions (Stronach 1984; Hall 1985, 1991; Hall and Neuman 1989; Ross and Bustin 2006; Martindale and Aberhan 2017; Martindale et al. 2017; Them et al. 2017a, 2018). The beds in this interval are finely laminated and lack major sedimentary structures (Hall 1987), indicating that they were deposited below fair weather wave base (Stronach 1984). Fossils exhibit little evidence of reworking or fragmentation (Martindale and Aberhan 2017), and the presence of articulated skeletons and carapaces (Figs. 3N-3P, 3R-3T, 13A), which become disarticulated after prolonged decay and transport, indicate that the organisms at Ya Ha Tinda did not drift or travel very far after they died. Instead, they quickly reached the seafloor and were buried by fine-grained sediment. Coleoid mantle remains preserved as non-mineralized impressions in fine-grained siliciclastic rock (Fig. 15A, 15B, 15D) suggest that some of the fossils experienced rapid burial, as such impressions are often found in event beds (Muscente and Allmon 2013). Altogether, these observations demonstrate that the organisms lived and were preserved where they died. Many substrates, including the coleoid gladii and crustacean carapaces, underwent phosphatization soon after burial and prior to burial compaction, leading to the retention of topographic relief on a sub-millimeter scale.

Fossil phosphatization occurs in environments conducive to phosphogenesis, or the early diagenetic precipitation of calcium phosphate minerals in sediments (Zhang et al. 1998; Muscente et al. 2015a). In addition to phosphatized fossils, phosphogenesis may produce phosphorites and other phosphatic facies (Glenn et al. 1994). Phosphogenic environments develop in places where a variety of physical and biogeochemical phenomena contribute to the development of sediment pore water with a high concentration of dissolved phosphate (Fig. 18). These phenomena include basin-scale processes that enhance phosphate availability, meso-scale processes that facilitate phosphorus burial, and localized pore water conditions that promote phosphorus remineralization, phosphate enrichment, and mineral precipitation (Glenn et al. 1994; Muscente et al. 2015a).

During the Early Jurassic in Alberta, phosphogenesis may have been fueled by oceanic upwelling of deep nutrient-rich seawater to the west and delivery of weathering-derived phosphate from the continent located to the east (Fig. 18A–18C). Phosphogenic environments often develop in zones of oceanic upwelling (Glenn et al. 1994), and Sinemurian phosphorites in southeastern British Columbia suggest that upwelling of the Panthalassa Ocean provided phosphate to shelf environments in Alberta during the Early Jurassic (Christie 1989; Poulton and Aitken 1989; Hall et al. 1998). This upwelling may have contributed to the long-lived exceptional preservational conditions that developed at Ya Ha Tinda. This conclusion does not rule out the possibility that other phenomena may have

conditions favored the burial of phosphorus, which had become trapped in the basin by anoxia. **D)** Geochemical gradients, reactions, and related processes during times when the environment (A, C) was most conducive to seafloor colonization, fossil phosphatization, and the burial of apatite minerals $(CaPO_4)$.

contributed to phosphatization at Ya Ha Tinda. Although phosphorus burial rates were low in the Early Jurassic (Cook and McElhinny 1979), the ocean likely contained a high concentration of phosphate in the Toarcian. Numerical models, osmium isotopes, and other detrital proxies suggest that weathering rates were high during the OAE (Montero-Serrano et al. 2015; Them et al. 2017b), perhaps two to five times greater than they were prior to the event (Them et al. 2017b). Under these circumstances, climactic warming may have caused the Toarcian OAE and associated carbon isotope excursion by increasing the delivery of nutrients to the ocean, thereby stimulating bioproductivity, expanding oxygen minimum zones, and favoring organic matter burial (Them et al. 2017b). Thus, continental weathering likely controlled the flux of phosphate to marine environments during the Pliensbachian—Toarcian transition.

Phosphorus enters sediment through burial of phosphatic skeletons, authigenic apatite, organic matter, and iron oxide particulates (Fig. 18D). Phosphogenesis then occurs when sedimentary processing of the phosphorus pushes pore water phosphate concentration beyond its ordinary supersaturation level with respect to apatite, allowing calcium phosphate minerals to precipitate. Although the Fernie Formation contains phosphatic skeletons (Figs. 5, 7–10) and phosphatic pebbles at some levels (Hall et al. 1998), these components contribute very little mass to the Red Deer and Poker Chip Shale members. Given that they consist of apatite biominerals, the crustacean carapaces and vertebrate skeletons may have provided the material and phosphate for their own mineralization (Martill 1988; Briggs and Kear 1994). Other sources of phosphate likely contributed to the preservation of the coleoid gladii, which were originally non-mineralized and contained no minerals. The largest fractions of pore water phosphate typically come from phosphorus remineralized from organic matter and desorbed from iron-(oxyhydr)oxide (FeOOH) particulates (Filippelli 1997). These processes, therefore, likely helped to promote fossil phosphatization at Ya Ha Tinda.

The Red Deer and Poker Chip Shale members contain little evidence of bioturbation (i.e., sediment mixing) outside of a few bioturbated layers (Fig. 2), suggesting that environments at Ya Ha Tinda conformed to simple models of chemically stratified sediments with microbial zonation (Callow and Brasier 2009). Beginning at the top of the water column and proceeding down through the sediment (Fig. 18D), microorganisms would have utilized the following oxidants as electron acceptors in their metabolic pathways of respiration: oxygen, nitrate, manganese, iron, sulfate, and carbon dioxide (van Gemerden 1993; Lyons et al. 1996). All of these metabolic pathways contribute to the remineralization of phosphorus. However, in modern settings, phosphogenesis tends to occur as a result of phosphorus remineralization via microbial sulfate reduction (Arning et al. 2009), an anaerobic process that occurs just below the redox boundary between suboxic and anoxic conditions. When FeOOH particulates with absorbed phosphate pass below this boundary, the reduction of FeOOH to ferrous iron results in the liberation of additional phosphate (O'Brien et al. 1990; Glenn et al. 1994; Okubo et al. 2018). Here, the efflux of phosphate from pore water to bottom water is also limited, in part, by reabsorption of phosphate onto FeOOH buried above the boundary (Fig. 18D). This reabsorption allows for a cyclical process, called 'iron pumping,' wherein FeOOH particulates shuttle phosphate into sediment and prevent its escape. Once released below the sediment-water interface, phosphate becomes partitioned between pore water and surface adsorption sites (Sunby et al. 1992; Paytan and McLaughlin 2007). Sediment pore water phosphate concentration, consequently, is a function of adsorption site availability and sedimentation rate (Glenn et al. 1994; Filippelli 1997). For this reason, phosphatization may have occurred in the sediment-starved environment at Ya Ha Tinda in the Early Jurassic, when sedimentation rates were low and siliciclastic deposition did not dilute buried organic matter or FeOOH particulates (Fig. 18B, 18C). Because sulfate and FeOOH reduction are redox-sensitive processes, the conditions that most favored phosphatization likely developed at Ya Ha Tinda during times of bottom water oxygenation, when animals inhabited seafloor environments located above the redox boundary and the zone of phosphogenesis.

In this context, we propose that the fossils of the Konservat-Lagerstätte were not preserved during the prolonged periods of euxinia implied by geochemical data, but rather, during the brief episodes of bottom water oxia and/or dysoxia recorded in the fossil record (Martindale and Aberhan 2017). During the euxinic periods, when the redox boundary was located above the sediment-water interface (Them et al. 2018), bottom water anoxia likely limited phosphorus burial and fossil phosphatization (Fig. 18B), as it promotes phosphate release from sediment and phosphorus recycling in the ocean (Meyer and Kump 2008; Watson et al. 2017). Even so, these periods may have indirectly contributed to fossil phosphatization by trapping nutrients provided by continental weathering and oceanic upwelling in basin seawater, thereby setting the stage for phosphatization. When oxygen levels increased on the seafloor (Fig. 18A, 18C), the foci of sulfate and FeOOH reduction shifted into the sediment (Fig. 18D), releasing phosphate to pore water and enhancing phosphorus burial. At the same time, the development of oxic bottom water allowed for the establishment of mixed pelagic-benthic communities of animals (Fig. 18D), which were ultimately buried in the sediment and mineralized in the phosphogenesis zone (Muscente et al. 2015a).

Other redox-sensitive processes may have also contributed to phosphatization at Ya Ha Tinda. When hydrogen sulfide becomes available, for example, sulfur-oxidizing bacteria living just above the redox boundary metabolize polyphosphates stored in their internal vacuoles and release phosphate (Brock and Schulz-Vogt 2011). This polyphosphate metabolism can, under some circumstances, force pore water phosphate concentrations beyond typical supersaturation levels and drive phosphorus mineralization (Schulz et al. 1999; Schulz and Schulz 2005; Arning et al. 2008, 2009; Goldhammer et al. 2010). In the case of Ya Ha Tinda, where the environment likely oscillated between euxinic and oxic conditions, sulfuroxidizing bacteria may have played a key role in controlling pore water phosphate concentrations.

Other Taphonomic and Diagenetic Processes

The minerals and materials found in the phosphatized fossils at Ya Ha Tinda formed in a number of different ways. The carbonaceous material likely represents organic matter, which is common in many types of skeletal and exceptionally preserved fossils (Muscente et al. 2017a). In most cases, organic preservation follows the collapse and concomitant coalescence of multiple tissues (Rex and Chaloner 1983; Rex 1986; Martí Mus 2014), and involves diagenetic polymerization of biomacromolecules into long-chain aliphatic components (Stankiewicz et al. 2000). Thus, the fossils may contain organic remains of the organisms. Although we cannot entirely rule out the possibility that the carbonaceous material was introduced into the fossils through migration of kerogen in the black shale, this explanation does not account for the presence of uniform carbonaceous layers within fossils of crustacean appendages (Fig. 12C-12R, 13E-13G, 13O-13U). In this case, the carbonaceous material may represent a waxy epicuticle or a non-biomineralized procuticle layer. Alternatively, such uniform carbonaceous layers may have formed through taphonomic demineralization of organic-rich phosphatic material (Muscente and Xiao 2015a). Of course, this interpretation may also imply that the carbonaceous material came from the organism. Future work should aim to ascertain the origin of the carbonaceous material and analyze its properties.

The aluminosilicate veneers found on the carbonaceous and phosphatic material at Ya Ha Tinda (Figs. 10B, 16A) resemble features of carbonaceous compressions and other fossils preserved with clays (Orr et al. 1998, 2009; Gabbott et al. 2001; Anderson et al. 2011; Cai et al. 2012; Muscente and Xiao 2015b; Muscente et al. 2016). Fossil aluminosilicification remains a topic of debate and may ultimately have

different root causes in different settings. In the case of fossils from the Burgess Shale, evidence suggests that late-stage volatization of carbonaceous material drove the emplacement of sheet silicate minerals (Orr et al. 1998; Butterfield et al. 2007). Although this explanation does not account for all examples of aluminosilicification (Gabbott et al. 2001; Anderson et al. 2011; Cai et al. 2012), it may explain the aluminosilicate veneers found on many organically preserved fossils (Page et al. 2008; Muscente et al. 2016), including those from the Fernie Formation. In the Fernie Formation, the aluminosilicate minerals occur on the exterior surfaces of carbonaceous and phosphatic fossils, indicating that they post-date the processes of phosphatization and organic preservation. They do not make up any fossil substrates (e.g., coleoid gladii or crustacean carapace), and therefore, do not represent authigenic clays. Accordingly, they likely formed through modification of the preexisting materials and surfaces, perhaps through thermal alteration. In any case, the aluminosilicate veneers do not provide insights into the properties of the organisms.

Phosphatized fossils, like those at Ya Ha Tinda, often contain calcite (Briggs and Wilby 1996). Petrographic, experimental, and geochemical data indicate that such calcite generally forms in the sediment as a consequence of microbial processes (Briggs and Kear 1994; Briggs and Wilby 1996; Schiffbauer et al. 2014b), such as iron reduction, sulfate reduction, or methanogenesis (Muscente et al. 2017b). These sorts of processes drive calcium carbonate precipitation by directly and indirectly producing bicarbonate, and consequently, increasing pore water alkalinity (Fig. 18D). In addition, these processes influence pore water pH. Although pore water is supersaturated with respect to apatite in most marine environments with oxic or dysoxic bottom water (Föllmi 1996), the rate of calcium phosphate precipitation at typical seawater pH (pH = 8.2) is usually low due to kinetic factors and the high ambient concentration of bicarbonate, which sequesters calcium through precipitation of calcite (Allison 1988b; Briggs and Wilby 1996). Pore water pH is generally lowest between the aerobic respiration and sulfate reduction zones because reactions (e.g., methanogenesis) in deeper microbial zones contribute only to alkalinity and buffer pH reduction (Callow and Brasier 2009). For this reason and others (see discussion above), phosphatization occurs around the redox boundary (Muscente et al. 2015a), where carbon dioxide and hydrogen sulfide produced by aerobic respiration, microbial sulfate reduction, and other processes result in low pH conditions that destabilize calcite, thereby favoring calcium phosphate over calcium carbonate (Lucas and Prevot 1991; Sagemann et al. 1999; Briggs 2003). Fossil calcification, in turn, occurs below the redox boundary after phosphatization (Schiffbauer et al. 2014b). Overall, this sequence of events may apply to the fossils at Ya Ha Tinda, where crustacean carapaces and coleoid gladii were first phosphatized and then overgrown by calcite crusts (Figs. 11D, 12C, 12D, 13B-13D, 14G, 14H, 16A, 16B).

The sphalerite and pyrite in the black shales at Ya Ha Tinda likely formed in response to microbial sulfate reduction (Fig. 18D). Sulfatereducing microorganisms oxidize organic matter and obtain energy by using sulfate (rather than oxygen) as an electron acceptor (Berner 1970, 1984). Sulfate reduction produces hydrogen sulfide, which may react with circumambient zinc or iron to precipitate sulfide minerals like sphalerite (Haymon et al. 1984; Spjeldnaes 2002; Hawkins et al. 2018) and pyrite (Briggs et al. 1996; Guan et al. 2016). The sphalerite cements surrounding some fossils at Ya Ha Tinda (Figs. 10C, 16A, 16B) likely formed around grains of sediments, perhaps from hydrogen sulfide produced as a byproduct of focused degradation of the fossils. Conversely, the framboidal pyrite (Fig. 9D) in the Red Deer and Poker Chip Shale members likely formed in the sediment (Berner 1970, 1984) and in the water column during periods of bottom water euxinia (Them et al. 2018). On rare occasions, when decaying animals provided nucleation sites and/or organic matter (Muscente and Xiao 2015a), microbial sulfate reduction resulted in mineralization of substrates with pyrite and/or sphalerite (Figs. 5D, 16B).

Unlike pyrite and sphalerite, the gypsum at Ya Ha Tinda likely precipitated during recent weathering (Fig. 5F–5H). The Red Deer and Poker Chip Shale members were deposited below fair weather wave base, rather than in shallow, evaporative environments that typically produce gypsum (Murray 1964). Gypsum occurs in close association with pyritized shells (Fig. 5), suggesting that calcium sulfate precipitation followed pyrite oxidation and the dissolution of calcium carbonate and calcium phosphate minerals (Ritsema and Groenenberg 1993). Thus, the gypsum manifests as a consequence of chemical weathering in the black shale (Martens 1925).

Although most of the exceptionally preserved fossils at Ya Ha Tinda contain barite (Figs. 5–16), its origin is unclear. Sedimentary barite forms via biogenic, hydrothermal, cold seep, and diagenetic pathways in modern marine environments (Raiswell et al. 2002; Griffith and Paytan 2012). Minerals formed via these pathways can be distinguished, to a degree, by their crystal sizes and morphologies (Paytan et al. 2002; Griffith and Paytan 2012). Biogenic barite, which occurs as ellipsoidal crystals <5 μm in diameter, forms within planktonic organisms and in microenvironments near decaying organic matter (Paytan et al. 2002). Hydrothermal and diagenetic barites, conversely, occur as bladed, tabular crystals (<20 µm in diameter) often in rosettes and diamond-shaped clusters (Paytan et al. 2002). The Ya Ha Tinda barite most closely resembles hydrothermal and diagenetic barite in terms of crystal size and shape (Figs. 5E, 5G, 8E-8F, 10A-10C). Given that the Fernie Formation does not contain significant evidence of hydrothermal or volcanic influence outside of a few minor ash beds and that the lath-shaped barite in the Red Deer Member at Scalp Creek likely formed through alteration of gypsum by barium-rich fluid (Fig. 2), the mineral may represent a diagenetic origin. If so, it may have precipitated on fossils as a result of sedimentary processing of biogenic barite around the sulfate reduction zone. In this zone, biogenic barite dissolves, leading to accumulation of barium in sulfate-depleted pore water. Barite then may re-precipitate where the barium-rich, sulfatedepleted water mixes with sulfate-rich fluid from above the sulfate reduction zone (Bolze et al. 1974; Brumsack and Gieskes 1983; Paytan et al. 2002; Griffith and Paytan 2012). This scenario explains the close association of barite with pyritized fossils (Fig. 5G) and sphalerite cements (Figs. 10C, 16A, 16B), and is consistent with interpretations of barite reported from fossils at other sites (Zabini et al. 2012; Muscente and Xiao 2015a). The barite, alternatively, may have formed in response to a drop in barite solubility with diagenetic changes in fluid pressures and temperatures and/or oxidative weathering of pyrite in the black shale by Ba-rich fluid (Hanor 2000; Broce and Schiffbauer 2017). These hypotheses require testing with additional analyses, perhaps ones focused on the sulfur isotope geochemistry of the sulfur-containing minerals.

Significance for Other Lagerstätten

In addition to the exceptionally preserved fossils at Ya Ha Tinda (Martindale et al. 2017), Toarcian strata contain the Posidonia Shale (Seilacher 1990; Röhl et al. 2001) and Strawberry Bank (Beacon Limestone Formation) Konservat-Lagerstätten (Williams et al. 2015) as well as a number of other deposits in Europe with insects, coleoids, fish, and marine reptiles (Ansorge 2003). In terms of facies, Ya Ha Tinda appears most similar to the Posidonia Shale (Martindale et al. 2017). Whereas the lower Fernie Formation and Posidonia Shale were deposited in deep marine systems, the Strawberry Bank and other Lagerstätten formed in nearshore settings (Williams et al. 2015), potentially in environments with brackish water (Ansorge 2003). Most of the exceptionally preserved fossils in these nearshore facies occur in limestones or calcareous concretions (Ansorge 2003; Williams et al. 2015), which may contain phosphatized tissues with three-dimensional relief (Williams et al. 2015). Fossils also occur in nodules of the Posidonia Shale (Seilacher 1990). Nonetheless, the Ya Ha Tinda and Posidonia Shale fossils were typically compacted and preserved as articulated skeletons and phosphatized

remains in bituminous shales intercalated with limestones (Seilacher 1982, 1990; Röhl et al. 2001; Gale and Schweigert 2016; Martindale et al. 2017). Facies and geochemical analyses indicate that the Posidonia Shale, like the lower Fernie Formation, was deposited under fluctuating, albeit predominantly euxinic, redox conditions (Röhl et al. 2001; Them et al. 2018). At this time, however, there is no empirical evidence of bottom water anoxia associated with the nearshore facies. Thus, the shallow- (Strawberry Bank) and deep-water (Ya Ha Tinda and Posidonia Shale) fossils were preserved through alternative preservational pathways in notably different depositional environments.

The most striking difference between the Posidonia Shale and Ya Ha Tinda Lagerstätten pertains to pyritized fossils. Although pyritized fossils are fairly common in the Posidonia Shale (Hudson 1982; Littke et al. 1991; Montero-Serrano et al. 2015), few such specimens have been collected from the lower Fernie Formation. The paucity of such fossils may represent a consequence of any number of factors. In general, pyrite formation varies with the concentration and availability of organic matter, sulfate, and reactive iron (Berner 1970, 1984). Factors that influence these variables around carcasses, such as redox conditions and sedimentation rate, control the likelihood and magnitude of fossil pyritization (Schiffbauer et al. 2014b). Fossil preservation through pyritization requires that microbial sulfate reduction and mineralization proceed rapidly enough to conserve organic substrates rather than simply destroy them (Briggs et al. 1996; Briggs 2003). Work on exceptionally preserved fossils suggests that, during the Phanerozoic, organisms were typically pyritized after rapid burial in fine-grained sediments with low concentrations of organic matter and high concentrations of reactive iron and sulfate (Briggs et al. 1991, 1996; Raiswell et al. 2008; Guan et al. 2016). In these sediments, most organic matter resides in carcasses, and their focused degradation via microbial sulfate reduction results in the development of circumambient microenvironments with sulfate, hydrogen sulfide, and reactive iron concentration gradients that kinetically and thermodynamically favor pyrite formation on biologic substrates (Briggs et al. 1996). At Ya Ha Tinda, such microenvironments may have developed infrequently because organic carbon burial rates were high (i.e., carcasses did not act as focal points of microbial sulfate reduction) or euxinic bottom water sequestered reaction iron, keeping its concentration at insufficient levels for pyritization. Of course, the Posidonia Shales also experienced high organic carbon burial and euxinic bottom water (Them et al. 2018), so these explanations do not account for the whole story.

During the OAE, environments with oxic or dysoxic bottom water may have been most favorable to pyritization, as their sediments contain the steepest gradients in sulfate, hydrogen sulfide, and reactive iron concentrations (Guan et al. 2016). Accordingly, the relative frequency of pyritized fossils in the Posidonia Shale may indicate that the unit was deposited under more frequent or pronounced episodes of seafloor oxygenation. Different sedimentation rates might also help to explain the difference in Lagerstätten. On an oxygenated seafloor, the amount of time that a carcass spends in the sulfate reduction zone of the sediment will ultimately affect its degree of pyritization (Schiffbauer et al. 2014b). The paucity of pyritized fossils at Ya Ha Tinda may indicate that sedimentation rates were too low for pyritization, such that, non-biomineralized tissues were generally destroyed before reaching the sulfate reduction zone and organic matter was too common in the sediment for pyritization of shells. In any case, future work on the sedimentology of the units may shed light on the issue.

All three of the major Konservat-Lagerstätten preserved during the Toarcian OAE—the deposits in the Fernie Formation, Posidonia Shale, and Beacon Limestone Formation—share a common element: phosphatized tissues and substrates. Some of these tissues and substrates originally consisted of phosphatic material (Figs. 5, 7–10), but all three deposits contain evidence of phosphatization (Seilacher et al. 1985; Williams et al. 2015; Martindale et al. 2017), and it is possible (if not likely) that this

process contributed to the preservation of skeletal elements as well (Gale and Schweigert 2016), altering their mineralogy. The presence of phosphatized fossils in all of these Lagerstätten may simply be a coincidence, but we prefer the interpretation that they share their origin with the OAE itself. Like the OAE (Montero-Serrano et al. 2015; Them et al. 2017b), environments conducive to phosphatization probably developed in response to a climactic warming event that enhanced continental weathering and phosphorus delivery to the ocean. The delivery of phosphorus did not directly promote phosphogenesis, as bioproductivity fueled by the input of nutrients caused anoxia to develop and substrates to release phosphate. Instead, phosphatization occurred on a limited scale within and near anoxic basins, which acted as phosphate traps. When oxic conditions arose on the seafloor, they were colonized by benthic and infaunal animals, which along with pelagic organisms, were phosphatized in the sediment. This interpretation reconciles the observation that anoxia does not guarantee conservation of non-biomineralized tissues (Allison 1988c) with the empirical relationship between Konservat-Lagerstätten and OAEs (Muscente et al. 2017b). Oceanic anoxia does not simply limit fossil fragmentation and degradation; it also breeds conditions conducive to authigenic mineralization of fossils buried along the fluctuating boundaries of oxygen minimum zones that expand and contract over time (Fig. 18A-

CONCLUSIONS

In summary, we investigated the preservation of fossils in the Konservat-Lagerstätte in the lower part of the Jurassic Fernie Formation at Ya Ha Tinda Ranch (Alberta, Canada) in order to explore the relationship between oceanic anoxia and exceptional fossil preservation. The fossils of articulated skeletons and soft tissues at Ya Ha Tinda were deposited during the Pliensbachian and Toarcian stages, including the time of the Toarcian OAE (~183 Ma), and include crustacean cuticles, coleoid gladii with ink sacs and mantle tissues, and articulated skeletons of fish, crinoids, and ichthyosaurs. In general, the fossils consist of phosphatic and carbonaceous materials associated with a variety of auxiliary minerals, including pyrite, calcite, barite, sphalerite, gypsum, and aluminosilicate clays. Evidently, the preservational pathway primarily involved phosphatization of skeletal and recalcitrant tissues. Although redox proxies indicate that euxinic bottom water was common in the area through the depositional history of the unit, this interpretation of the geochemical data does not concur with observations of the fossils. Prolonged periods of seafloor anoxia would have been inhospitable to benthic lifeforms and resulted in phosphate release from the sediment, thereby limiting the potential for phosphatization. Indeed, the interval of supposed anoxia contains burrows, benthic animal fossils, and phosphatized remains at multiple levels. We attribute this discrepancy to the different timescales of geochemical and paleontological data, and propose that the fossils were preserved during brief episodes of seafloor oxygenation, when the environment would have been most favorable to benthic communities and phosphate mineralization. Phosphatization was likely fueled by phosphate delivery from continental weathering, ocean upwelling, and/or nutrient trapping within the anoxic basin. Altogether, these results account for the observation that oceanic anoxia leads to exceptional fossil preservation (Muscente et al. 2017b). Although anoxia does not guarantee survival of non-biomineralized tissues or articulated skeletons, as anaerobic metabolic processes can degrade soft tissue as rapidly as aerobic decay (Allison 1988c), our work suggests that it contributes to the development of conditions conducive to authigenic mineralization. Oxygen minimum zones do not, by themselves, lead to exceptional fossil preservation. Instead, exceptional fossil preservation during OAEs reflects the interplay of two factors: anoxia limiting the degradation of organisms via scavenging and the broad-scale development of geochemical gradients that allow for fossil mineralization along expanding and contracting oxygen minimum zones.

ACKNOWLEDGMENTS

This research was supported by a grant from the National Science Foundation (NSF EAR award #1660005) and an internal UT Austin Jackson School of Geosciences seed grant to RCM. JDS is supported by NSF EAR awards #1652351 and #1636643. We thank Rick and Jean Smith, the Ya Ha Tinda Ranch caretakers, as well as David Gummer, Susan Hairsine, Derek Petersen, Bill Perry, and Gloria Sundbo at Parks Canada for research permits and logistical support (Permit #YHTR-2014-16156). In addition, would like to thank Don Brinkman, Graeme Housego, Jim McCabe, Rhian Russell, Dan Spivak, Brandon Strilisky, and Darren Tanke at the Royal Tyrrell Museum of Palaeontology for their aid with permits, logistical support, and fossil curation (Permits: #13-058, #14-009, #15-019, #16-063, #17-048, and #18-072). We would also like to thank Angela Gerhardt, Ben Gill, Josh Lively, Selva Marroquín, Teddy Them, Emma Tulsky, Jason Visser, and Keith Minor as well as Bill and Serena Martindale for assistance in the field. Finally, we would like to thank Tom Etzel and James Maner for their support with electron imaging and elemental analysis at UT Austin. Marc Laflamme and an anonymous reviewer are thanked for their helpful comments to the manuscript.

REFERENCES

- AL-SUWAIDI, A.H., JENKYNS, H.C., HESSELBO, S.P., ANGELOZZI, G.N., BAUDIN, F., RICCARDI, A.C., MANCENIDO, M.O., AND DAMBORENEA, S.E., 2010, First record of the early Toarcian Oceanic Anoxic Event from the Southern Hemisphere, Neuquén Basin, Argentina: Journal of the Geological Society, v. 167, p. 633–636, doi: 10.1144/0016-76492010-025.
- ALLISON, P., 1988a, Phosphatized soft-bodied squids from the Jurassic Oxford Clay: Lethaia, v. 21, p. 403–410.
- Allison, P.A., 1988b, Konservat-Lagerstätten: cause and classification: Paleobiology, v. 14, p. 331–344, doi: 10.2307/2400942.
- Allison, P.A., 1988c, The role of anoxia in the decay and mineralization of proteinaceous macro-fossils: Paleobiology, v. 14, p. 139–154.
- ALLISON, P.A. AND BRIGGS, D.E.G., 1993, Exceptional fossils record: distribution of soft-tissue preservation through the Phanerozoic: Geology, v. 21, p. 527–530.
- Anderson, E., Schiffbauer, J.D., and Xiao, S., 2011, Taphonomic study of Ediacaran organic-walled fossils confirms the importance of clay minerals and pyrite in Burgess Shale-type preservation: Geology, v. 39, p. 643–646.
- Anderson, R.P., Tosca, N.J., Gaines, R.R., Mongiardino Koch, N., and Briggs, D.E.G., 2018, A mineralogical signature for Burgess Shale-type fossilization: Geology, v. 46, p. 347–350, doi: 10.1130/g39941.1.
- Ansorge, J., 2003, Insects from the lower Toarcian of Middle Europe and England: Acta Zoologica Cracoviensia, v. 46, p. 291–310.
- Arning, E.T., Birgel, D., Brunner, B., and Peckmann, J., 2009, Bacterial formation of phosphatic laminites off Peru: Geobiology, v. 7, p. 295–307, doi: 10.1111/j.1472-4669.2009.00197.x.
- Arning, E.T., Birgel, D., Schulz-Vogt, H.N., Holmkvist, L., Jørgensen, B.B., Larson, A., and Peckmann, J., 2008, Lipid biomarker patterns of phosphogenic sediments from upwelling regions: Geomicrobiology Journal, v. 25, p. 69–82, doi: 10.1080/01490450 801934854.
- Balthasar, U., 2007, An early Cambrian organophospathic brachiopod with calcitic granules: Palaeontology, v. 50, p. 1319–11325, doi: 10.1111/j.1475-4983.2007.00729.x.
- Beerling, D.J. and Brenthall, S.J., 2007, Numerical evaluation of mechanisms driving Early Jurassic changes in global carbon cycling: Geology, v. 35, p. 247–250, doi: 10.1130/g23416a.1.
- BERNER, R.A., 1970, Sedimentary pyrite formation: American Journal of Science, v. 268, p. 1–23, doi: 10.2475/ajs.268.1.1.
- Berner, R.A., 1984, Sedimentary pyrite formation: an update: Geochimica et Cosmochimica Acta, v. 48, p. 605–615, doi: 10.1016/0016-7037(84)90089-9.
- Bolze, C.E., Malone, P.G., and Smith, M.J., 1974, Microbial mobilization of barite: Chemical Geology, v. 13, p. 141–143, doi: 10.1016/0009-2541(74)90006-0.
- BRIGGS, D.E.G., 2003, The role of decay and mineralization in the preservation of soft-bodied fossils: Annual Review of Earth and Planetary Sciences, v. 31, p. 275–301 doi: 10.1146/annurev.earth.31.100901.144746.
- BRIGGS, D.E.G., BOTTRELL, S.H., AND RAISWELL, R., 1991, Pyritization of soft-bodied fossils: Beecher's Trilobite Bed, Upper Ordovician, New York State: Geology, v. 19, p. 1221–1224.
- BRIGGS, D.E.G. AND KEAR, A.J., 1994, Decay and mineralization of shrimps: PALAIOS, v. 9, p. 431–456.
- BRIGGS, D.E.G., KEAR, A.J., MARTILL, D.M., AND WILBY, P.R., 1993, Phosphatization of soft-tissue in experiments and fossils: Journal of the Geological Society, London, v. 150, p. 1035–1038.
- BRIGGS, D.E.G., RAISWELL, R., BOTTRELL, S.H., HATFIELD, D., AND BARTELS, C., 1996, Controls on the pyritization of exceptionally preserved fossils: an analysis of the Lower Devonian Hunsrück Slate of Germany: American Journal of Science, v. 296, p. 633–663.

- BRIGGS, D.E.G. AND WILBY, P.R., 1996, The role of calcium carbonate-calcium phosphate switch in the mineralization of soft-bodied fossils: Journal of the Geological Society, London, v. 153, p. 665–668.
- Broce, J.S. and Schiffbauer, J.D., 2017, Taphonomic analysis of Cambrian verminform fossils of Utah and Nevada, and implications for the chemistry of Burgess Shale-tye preservation: PALAIOS, v. 32, p. 600–619, doi: 10.2110/palo.2017.011.
- Brock, J. and Schulz-Vogt, H.N., 2011, Sulfide induces phosphate release from polyphosphate in cultures of a marine Beggiatoa strain: ISME Journal, v. 5, p. 497–506.
- Brumsack, H.J. and Gieskes, J.M., 1983, Interstitial water trace-metal chemistry of laminated sediments from the Gulf of California, Mexico: Marine Chemistry, v. 14, p. 89–106, doi: 10.1016/0304-4203(83)90072-5.
- BUTTERFIELD, N.J., 1995, Secular distribution of Burgess Shale-type preservation: Lethaia, v. 28, p. 1–13.
- BUTTERFIELD, N.J., 2003, Exceptional fossil preservation and the Cambrian Explosion: Integrative and Comparative Biology, v. 43, p. 166–177.
- BUTTERFIELD, N.J., 2012, Does cement-induced sulfate limitation account for Burgess Shale-type preservation?: Proceedings of the National Academy of Sciences of the United States of America, v. 109, p. E1901–E1901, doi: 10.1073/pnas.1206878109.
- BUTTERFIELD, N.J., BALTHASAR, U., AND WILSON, L.A., 2007, Fossil diagenesis in the Burgess Shale: Palaeontology, v. 50, p. 537–543.
- CAI, Y., SCHIFFBAUER, J.D., HUA, H., AND XIAO, S., 2012, Preservational modes in the Ediacaran Gaojiashan Lagerstätte: pyritization, aluminosilicification, and carbonaceous compression: Palaeogeography, Palaeoclimatology, Palaeoecology, v. 326–328, p. 109– 117.
- Callow, R.H.T. and Brasier, M.D., 2009, Remarkable preservation of microbial mats in Neoproterozoic siliciclastic settings: implications for Ediacaran taphonomic models: Earth-Science Reviews, v. 96, p. 207–219, doi: 10.1016/j.earscirev.2009.07.002.
- CARUTHERS, A.H., GRÖCKE, D.R., AND SMITH, P.L., 2011, The significance of an Early Jurassic (Toarcian) carbon-isotope excursion in Haida Gwaii (Queen Charlotte Islands), British Columbia, Canada: Earth and Planetary Science Letters, v. 307, p. 19–26, doi: 10.1016/j.epsl.2011.04.013.
- CARUTHERS, A.H., SMITH, P.L., AND GRÖCKE, D.R., 2014, The Pliensbachian—Toarcian (Early Jurassic) extinction: a North American perspective, *in* G. Keller and A.C. Kerr (eds.), Volcanism, Impacts, and Mass Extinctions: Causes and Effects: Geological Society of America, Boulder, Colorado, Special Paper 505, p. 225–243.
- CASWELL, B.A. AND COE, A.L., 2014, The impact of anoxia on pelagic macrofauna during the Toarcian Oceanic Anoxic Event (Early Jurassic): Proceedings of the Geologists' Association, v. 125, p. 383–391, doi: 10.1016/j.pgeola.2014.06.001.
- CHRISTIE, R.L., 1989, Jurassic phosphorite of the Fernie synclinorium, southeastern British Columbia, Canada, in A.J.G. Nothold, R.P. Sheldon, and D.F. Davidson (eds.), Phosphate Deposits of the World: Phosphate Rock Resources: Cambridge University Press, New York, p. 79–83.
- Combes, C., Cazalbou, S., and Rey, C., 2016, Apatite biominerals: Minerals, v. 6, p. 1–25. Conway Morris, S., 1986, The community structure of the middle Cambrian Phyllopod bed (Burgess Shale): Palaeontology, v. 29, p. 423–467.
- СООК, P.J. AND McELHINNY, M.W., 1979, A reevaluation of the spatial and temporal distribution of sedimentary phosphate deposits in the light of plate tectonics: Economic Geology, v. 74, p. 315–330, doi: 10.2113/gsecongeo.74.2.315.
- Creveling, J.R., Johnston, D.T., Poulton, S.W., Kotrc, B., März, C., Schrag, D.P., and Knoll, A.H., 2014a, Phosphorus sources for phosphatic Cambrian carbonates: Geological Society of America Bulletin, v. 126, p. 145–163, doi: 10.1130/b30819.1.
- CREVELING, J.R., KNOLL, A.H., AND JOHNSTON, D.T., 2014b, Taphonomy of Cambrian phosphatic small shelly fossils: PALAIOS, v. 29, p. 295–308, doi: 10.2110/palo.2014.002
- CUSACK, M. AND WILLIAMS, A., 1996, Chemico-structural degradation of Carboniferous lingulid shells: Philosophical Transactions of the Royal Society of London, Series B, Biological Sciences, v. 351, p. 33–49, doi:10.1098/rstb.1996.0003.
- CUSACK, M., WILLIAMS, A., AND BUCKMAN, J.O., 1999, Chemico-structural evolution of linguloid brachiopod shells: Palaeontology, v. 42, p. 799–840, doi: 10.1111/1475-4983.00098.
- Danise, S., Twitchett, R.J., and Little, C.T.S., 2015, Environmental controls on Jurassic marine ecosystems during global warming: Geology, v. 43, p. 263–266, doi: 10.1130/g3 6390.1
- DOGUZHAEVA, L.A. AND MUTVEI, H., 2003, Gladius composition and ultrastructure in extinct squid-like coleoids: *Loligosepia*, *Trachyteuthis* and *Teudopsis*: Revue de Paleobiologie Genève, v. 22, p. 877–894.
- DONOVAN, D.T. AND TOLL, R.B., 1988, The gladius in coleoid (Cephalopoda) evolution, in M.R. Clarke and E.R. Trueman (eds.), Paleontology and Neontology of Cephalopods: Academic Press, London, p. 89–101.
- FELDMANN, R., 1989, Whitening fossils for photographic purposes: The Paleontological Society Special Publications, v. 4, p. 342–346.
- Feldmann, R.M. and Copeland, M.J., 1988, A new species of erymid lobster from Lower Jurassic strata (Sinemurian/Pliensbachian), Fernie Formation, southwestern Alberta: Geological Survey of Canada Bulletin, v. 379, p. 93–101, doi: 10.4095/126974.
- Feldmann, R.M., VILLAMIL, T., and Kauffman, E.G., 1999, Decapod and stomatopod crustaceans from mass mortality Lagerstätten: Turonian (Cretaceous) of Colombia: Journal of Paleontology, v. 73, p. 91–101.

- FILIPPELLI, G.M., 1997, Controls on phosphorus concentration and accumulation in oceanic sediments: Marine Geology, v. 139, p. 231–240, doi: 10.1016/S0025-3227(96)00113-2.
- FÖLLMI, K.B., 1996, The phosphorus cycle, phosphogenesis and marine phosphate-rich deposits: Earth-Science Reviews, v. 40, p. 55–124, doi: 10.1016/0012-8252(95)00049-6.
- FUCHS, D., IFRIM, C., AND STINNESBECK, W., 2008, A new palaeoctopus (Cephalopoda: Coleoidea) from the Late Cretaceous of Vallecillo, north-eastern Mexico, and implications for the evolution of Octopoda: Palaeontology, v. 51, p. 1129–1139, doi: 10.1111/j.1475-4983.2008.00797.x.
- GABBOTT, S.E., NORRY, M.J., ALDRIDGE, R.J., AND THERON, J.N., 2001, Preservation of fossils in clay minerals; a unique example from the Upper Ordovician Soom Shale, South Africa: Proceedings of the Yorkshire Geological Society, v. 53, p. 237–244, doi: 10.1144/pygs.53.3.237.
- GAINES, R.R. AND DROSER, M.L., 2010, The paleoredox setting of Burgess Shale-type deposits: Palaeogeography, Palaeoclimatology, Palaeoecology, v. 297, p. 649–661, doi: 10.1016/j.palaeo.2010.09.014.
- GAINES, R.R., DROSER, M.L., ORR, P.J., GARSON, D., HAMMARLUND, E., QI, C., AND CANFIELD, D.E., 2012a, Burgess shale-type biotas were not entirely burrowed away: Geology, v. 40, p. 283–286, doi: 10.1130/g32555.1.
- GAINES, R.R., HAMMARLUND, E.U., HOU, X., QI, C., GABBOTT, S.E., ZHAO, Y., PENG, J., AND CANFIELD, D.E., 2012b, Mechanism for Burgess Shale-type preservation: Proceedings of the National Academy of Sciences, v. 109, p. 5180–5184, doi: 10.1073/pnas.111178410
- GALE, A. AND SCHWEIGERT, G., 2016, A new phosphatic-shelled cirripede (Crustacea, Thoracica) from the Lower Jurassic (Toarcian) of Germany—the oldest epiplanktonic barnacle: Palaeontology, v. 59, p. 59–70, doi: 10.1111/pala.12207.
- GLASS, K., ITO, S., WILBY, P.R., SOTA, T., NAKAMURA, A., BOWERS, C.R., VINTHER, J., DUTTA, S., SUMMONS, R., BRIGGS, D.E.G., WAKAMATSU, K., AND SIMON, J.D., 2012, Direct chemical evidence for eumelanin pigment from the Jurassic period: Proceedings of the National Academy of Sciences, v. 109, p. 10218–10223, doi: 10.1073/pnas.1118448109.
- Glenn, C.R., Follmi, K.B., Riggs, S.R., Baturin, G.N., Grimm, K.A., Trappe, J., Abed, A.M., Galli-Olivier, C., Garrison, R.E., Ilyin, A.V., Jehl, C., Rohrlich, V., Sadaqah, R.M.Y., Schidlowski, M., Sheldon, R.E., and Siegmund, H., 1994, Phosphorus and phosphorites: sedimentology and environments of formation: Eclogae Geologicae Helvetiae, v. 87, p. 747–788.
- GOLDHAMMER, T., BRUCHERT, V., FERDELMAN, T.G., AND ZABEL, M., 2010, Microbial sequestration of phosphorus in anoxic upwelling sediments: Nature Geoscience, v. 3, p. 557–561, http://www.nature.com/ngeo/journal/v3/n8/suppinfo/ngeo913_S1.html.
- GOLDSTEIN, J., NEWBURY, D.E., ECHLIN, P., JOY, D.C., LYMAN, C.E., LIFSHIN, E., SAWYER, L., AND MICHAEL, J.R., 2003, Scanning Electron Microscopy and X-ray Microanalysis: third edition: Springer, New York, 689 p.
- Griffith, E.M. and Paytan, A., 2012, Barite in the ocean—occurrence, geochemistry and palaeoceanographic applications: Sedimentology, v. 59, p. 1817–1835, doi: 10.1111/j.13 65-3091.2012.01327.x.
- GRÖCKE, D.R., HORI, R.S., TRABUCHO-ALEXANDRE, J., KEMP, D.B., AND SCHWARK, L., 2011, An open ocean record of the Toarcian oceanic anoxic event: Solid Earth, v. 2, p. 245– 257. doi: 10.5194/se-2-245-2011.
- GUAN, C., WANG, W., ZHOU, C., MUSCENTE, A.D., WAN, B., CHEN, X., YUAN, X., CHEN, Z., AND OUYANG, Q., 2016, Controls on fossil pyritization: redox conditions, sedimentary organic matter content, and Chuaria preservation in the Ediacaran Lantian Biota: Palaeogeography, Palaeoclimatology, Palaeoecology, v. 474, p. 26–35, doi: 10.1016/j. palaeo.2016.05.013.
- HALL, R.L., 1985, Paraplesioteuthis hastata (Münster), the first teuthid squid recorded from the Jurassic of North America: Journal of Paleontology, v. 59, p. 870–874.
- HALL, R.L., 1987, New Lower Jurassic ammonite faunas from the Fernie Formation, southern Canadian Rocky Mountains: Canadian Journal of Earth Sciences, v. 24, p. 1688–1704, doi: 10.1139/e87-162.
- HALL, R.L., 1991, Seirocrinus subangularis (Miller, 1821), a Pliensbachian (Lower Jurassic) crinoid from the Fernie Formation, Alberta, Canada: Journal of Paleontology, v. 65, p. 300–307, doi: 10.1017/S0022336000020539.
- HALL, R.L., 2006, New, biostratigraphically significant ammonites from the Jurassic Fernie Formation, southern Canadian Rocky Mountains: Canadian Journal of Earth Sciences, v. 43, p. 555–570, doi: 10.1139/e06-004.
- HALL, R.L., McNicoll, V., Gröcke, D.R., Craig, J., and Johnston, K., 2004, Integrated stratigraphy of the lower and middle Fernie Formation in Alberta and British Columbia, Western Canada: Rivista Italiana di Paleontologia e Stratigrafia, v. 110, p. 61–68.
- HALL, R.L. AND NEUMAN, A.G., 1989, *Teudopsis cadominensis*, a new teuthid squid from the Toarcian (Lower Jurassic) of Alberta: Journal of Paleontology, v. 63, p. 324–327, doi: 10.1017/S0022336000019478.
- HALL, R.L., POULTON, T.P., AND MONGER, J.W.H., 1998, Field Trip A1: Calgary–Vancouver, in P.L. Smith (ed.), Field Guilde for the Fifth International Symposium on the Jurassic System: International Union of Geological Sciences Subcommission on Jurassic Stratigraphy, Vancouver, p. 29–61.
- HANOR, J.S., 2000, Barite-celestine geochemistry and environments of formation: Reviews in Mineralogy and Geochemistry, v. 40, p. 193–275, doi: 10.2138/rmg.2000.40.4.
- HAWKINS, A.D., LIU, H.P., BRIGGS, D.E.G., MUSCENTE, A.D., McKAY, R.M., WITZKE, B.J., AND XIAO, S., 2018, Taphonomy and biological affinitiy of three-dimensionally phosphatized bromalites from the middle Ordovician Winneshiek Lagerstätte, northeastern Iowa, USA: PALAIOS, v. 33, p. 1–15, doi: 10.2110/palo.2017.053.

- HAYMON, R.M., KOSKI, R.A., AND SINCLAIR, C., 1984, Fossils of hydrothermal vent worms from Cretaceous sulfide ores of the Samail Ophiolite, Oman: Science, v. 223, p. 1407– 1409, doi: 10.1126/science.223.4643.1407.
- HESSELBO, S.P., GRÖCKE, D.R., JENKYNS, H.C., BJERRUM, C.J., FARRIMOND, P., MORGANS BELL, H.S., AND GREEN, O.R., 2000, Massive dissociation of gas hydrate during a Jurassic oceanic anoxic event: Nature, v. 406, p. 392–395, doi: 10.1038/35019044.
- HUDSON, J.D., 1982, Pyrite in ammonite-bearing shales from the Jurassic of England and Germany: Sedimentology, v. 29, p. 639–667, doi: 10.1111/j.1365-3091.1982.tb00072.x.
- HUNT, S. AND NIXON, M., 1981, A comparative study of protein composition in the chitin-protein complexes of the beak, pen, sucker disc, radula and oesophageal cuticle of cephalopods: Comparative Biochemistry and Physiology Part B, Comparative Biochemistry, v. 68, p. 535–546, doi: 10.1016/0305-0491(81)90071-7.
- IFRIM, C., STINNESBECK, W., AND FREY, E., 2007, Upper Cretaceous (Cenomanian-Turonian and Turonian-Coniacian) open marine plattenkalk deposits in NE Mexico: Neues Jahrbuch für Geologie und Paläontologie Abhandlungen, v. 245, p. 71–81.
- IKOMA, T., KOBAYASHI, H., TANAKA, J., WALSH, D., AND MANN, S., 2003, Microstructure, mechanical, and biomimetic properties of fish scales from *Pagrus major*: Journal of Structural Biology, v. 142, p. 327–333, doi: 10.1016/S1047-8477(03)00053-4.
- JENKYNS, H.C., 1988, The early Toarcian (Jurassic) anoxic event: stratigraphic, sedimentary, and geochemical evidence: American Journal of Science, v. 288, p. 101– 151, doi: 10.2475/ajs.288.2.101.
- JENKYNS, H.C., 2010, Geochemistry of oceanic anoxic events: Geochemistry, Geophysics, Geosystems, v. 11, p. 1–30, doi: 10.1029/2009GC002788.
- KEMR, D.B. AND IZUMI, K., 2014, Multiproxy geochemical analysis of a Panthalassic margin record of the early Toarcian oceanic anoxic event (Toyora area, Japan): Palaeogeography, Palaeoclimatology, Palaeoecology, v. 414, p. 332–341, doi: 10.1016/j.palaeo.2014.09.019.
- KLUG, C., RIEGRAF, W., AND LEHMANN, J., 2012, Soft-part preservation in heteromorph ammonites from the Cenomanian–Turonian Boundary Event (OAE 2) in north-west Germany: Palaeontology, v. 55, p. 1307–1331, doi: 10.1111/j.1475-4983.2012.01196.x.
- KUNKEL, J.G., 2013, Modeling the calcium and phosphate mineralization of American lobster cuticle: Canadian Journal of Fisheries and Aquatic Sciences, v. 70, p. 1601–1611, doi: 10.1139/cjfas-2013-0034.
- KUNKEL, J.G., NAGEL, W., AND JERCINOVIC, M.J., 2012, Mineral fine structure of the American lobster cuticle: Journal of Shellfish Research, v. 31, p. 515–526, doi: 10.2 983/035.031.0211.
- Lathullière, B. and Marchal, D., 2009, Extinction, survival and recovery of corals from the Triassic to Middle Jurassic time: Terra Nova, v. 21, p. 57–66, doi: 10.1111/j.13 65-3121.2008.00856.x.
- LITTKE, R., LEYTHAEUSER, D., RULLKÖTTER, J., AND BAKER, D.R., 1991, Keys to the depositional history of the Posidonia Shale (Toarcian) in the Hils Syncline, northern Germany: Geological Society of London, Special Publications, v. 58, p. 311–333, doi: 10.1144/gsl.sp.1991.058.01.20.
- LITTLE, C.T.S. AND BENTON, M.J., 1995, Early Jurassic mass extinction: a global long-term event: Geology, v. 23, p. 495–498, doi: 10.1130/0091-7613(1995)023<0495: ejmeag>2.3.co;2.
- LUCAS, J. AND PREVOT, L.E., 1991, Phosphates and fossil preservation, in P.A. Allison and D.E.G. Briggs (eds.), Taphonomy: Releasing the Data Locked in the Fossil Record: Plenum Press, New York, p. 389–409.
- Lyons, W.B., Lent, R.M., Burnett, W.C., Chin, P., Landing, W.M., Orem, W.H., and McArthur, J.M., 1996, Jellyfish Lake, Palau: regeneration of C, N, Si, and P in anoxic marine lake sediments: Limnology and Oceanography, v. 41, p. 1394–1403.
- Marroquín, S.M., Martindale, R.C., and Fuchs, D., 2018, New records of the late Pliensbachian to early Toarcian (Early Jurassic) gladius-bearing coleoid cephalopods from the Ya Ha Tinda Lagerstätte, Canada: Papers in Palaeontology, v. 4, p. 245–276, doi: 10.1002/spp2.1104.
- Martens, J.H.C., 1925, Sulphate minerals from weathering of shale near Ithaca, New York: American Mineralogist, v. 10, p. 175–176.
- MARTÍ MUS, M., 2014, Interpreting 'shelly' fossils preserved as organic films: the case of hyolithids: Lethaia, v. 47, p. 397–404.
- Martill, D.M., 1988, Preservation of fish in the Cretaceous Santana Formation of Brazil: Palaeontology, v. 31, p. 1–18.
- MARTILL, D.M., IBRAHIM, N., BRITO, P.M., BAIDER, L., ZHOURI, S., LOVERIDGE, R., NAISH, D., AND HING, R., 2011, A new Plattenkalk Konservat Lagerstätte in the Upper Cretaceous of Gara Sbaa, south-eastern Morocco: Cretaceous Research, v. 32, p. 433–446, doi: 10.1016/j.cretres.2011.01.005.
- Martindale, R.C. and Aberhan, M., 2017, Response of macrobenthic communities to the Toarcian Oceanic Anoxic Event in northeastern Panthalassa (Ya Ha Tinda, Alberta, Canada): Palaeogeography, Palaeoclimatology, Palaeoecology, v. 478, p. 103–120, doi: 10.1016/j.palaeo.2017.01.009.
- Martindale, R.C., Them, T.R., Gill, B.C., Marroquín, S.M., and Knoll, A.H., 2017, A new Early Jurassic (ca. 183 Ma) fossil Lagerstätte from Ya Ha Tinda, Alberta, Canada: Geology, v. 45, p. 255–258, doi: 10.1130/g38808.1.
- MAXWELL, E.E. AND MARTINDALE, R.C., 2017, New Saurorhynchus (Actinopterygii: Saurichthyidae) material from the Early Jurassic of Alberta, Canada: Canadian Journal of Earth Sciences, v. 54, p. 714–719, doi: 10.1139/cjes-2017-0015.
- McElwain, J.C., Wade-Murphy, J., and Hesselbo, S.P., 2005, Changes in carbon dioxide during an oceanic anoxic event linked to intrusion into Gondwana coals: Nature, v. 435, p. 479–482, doi: 10.1038/nature03618.

- MEYER, K.M. AND KUMP, L.R., 2008, Oceanic euxinia in Earth history: causes and consequences: Annual Review of Earth and Planetary Sciences, v. 36, p. 251–288, doi: 10.1146/annurev.earth.36.031207.124256.
- MONTERO-SERRANO, J.-C., FOLLMI, K.B., ADATTE, T., SPANGENBERG, J.E., TRIBOVILLARD, N., FANTASIA, A., AND SUAN, G., 2015, Continental weathering and redox conditions during the early Toarcian Oceanic Anoxic Event in the northwestern Tethys: insight from the Posidonia Shale section in the Swiss Jura Mountains: Palaeogeography, Palaeoclimatology, Palaeoccology, v. 429, p. 83–99, doi: 10.1016/j.palaeo.2015.03.043.
- Moulin, M., Fluteau, F., Courtillot, V., Marsh, J., Delpech, G., Quidelleur, X., and Gérard, M., 2017, Eruptive history of the Karoo lava flows and their impact on early Jurassic environmental change: Journal of Geophysical Research, Solid Earth, v. 122, p. 738–772, doi: 10.1002/2016jb013354.
- Murray, R.C., 1964, Origin and diagenesis of gypsum and anhydrite: Journal of Sedimentary Research, v. 34, p. 512–523, doi: 10.1306/74d710d2-2b21-11d7-8648000102c1865d.
- Muscente, A.D. and Allmon, W.D., 2013, Revision of the hydroid *Plumalina* Hall, 1858 in the Silurian and Devonian of New York: Journal of Paleontology, v. 87, p. 710–725, doi: 10.1666/12-125.
- Muscente, A.D. Allmon, W.D., and Xiao, S., 2016, The hydroid fossil record and analytical techniques for assessing the affinities of putative hydrozoans and possible hemichordates: Palaeontology, v. 59, p. 71–87, doi: 10.1111/pala.12209.
- Muscente, A.D., Czaja, A.D., Riedman, L.A., and Colleary, C., 2017a, Organic matter in fossils, *in* W.M. White (ed.), Earth Science Series, Encylopedia of Geochemistry: Springer, Cham, Switzerland, p. 1–5, doi: 10.1007/978-3-319-39193-9.
- MUSCENTE, A.D., HAWKINS, A.D., AND XIAO, S., 2015a, Fossil preservation through phosphatization and silicification in the Ediacaran Doushantuo Formation (South China): a comparative synthesis: Palaeogeography, Palaeoclimatology, Palaeoecology, v. 434, p. 46–62, doi: 10.1016/j.palaeo.2014.10.013
- Muscente, A.D., Michel, F.M., Dale, J.G., and Xiao, S., 2015b, Assessing the veracity of Precambrian 'sponge' fossils using *in situ* nanoscale analytical techniques: Precambrian Research, v. 263, p. 142–156, doi: 10.1016/j.precamres.2015.03.010.
- Muscente, A.D., Schiffbauer, J.D., Broce, J., Laflamme, M., O'Donnell, K., Boag, T.H., Meyer, M., Hawkins, A.D., Huntley, J.W., McNamara, M., MacKenzie, L.A., Stanley Jr, G.D., Hinman, N.W., Hofmann, M.H., and Xiao, S., 2017b, Exceptionally preserved fossil assemblages through geologic time and space: Gondwana Research, v. 48, p. 164–188, doi: 10.1016/j.gr.2017.04.020.
- MUSCENTE, A.D. AND XIAO, S., 2015a, New occurrences of *Sphenothallus* in the lower Cambrian of South China: implications for its affinities and taphonomic demineralization of shelly fossils: Palaeogeography, Palaeoclimatology, Palaeoecology, v. 437, p. 141–146, doi: 10.1016/j.palaeo.2015.07.041.
- Muscente, A.D. and Xiao, S., 2015b, Resolving three-dimensional and subsurficial features of carbonaceous compressions and shelly fossils using backscattered electron scanning electron microscopy (BSE-SEM): PALAIOS, v. 30, p. 462–481 doi: 10.2110/palo.2014.094
- O'BRIEN, G.W., MILNES, A.R., WEEH, H.H., HEGGIE, D.T., RIGGS, S.R., CULLEN, D.J., MARSHALL, J.F., AND COOK, P.J., 1990, Sedimentation dynamics and redox iron-cycling: controlling factors for the apatite-glauconite association on the east Australian continental margin, *in* A.J.G. Notholt and I. Jarvis (eds.), Phosphorite Research and Development: Geological Society Special Publication 52, p. 61–86.
- OKUBO, J., MUSCENTE, A.D., LUVIZOTTO, G.L., UHLEIN, G.J., AND WARREN, L.V., 2018, Phosphogenesis, aragonite fan formation and seafloor environments following the Marinoan glaciation: Precambrian Research, v. 311, p. 24–36, doi: 10.1016/j.pre camres.2018.04.002.
- ONOZATO, H. AND WATABE, N., 1979, Studies on fish scale formation and resorption: Cell and Tissue Research, v. 201, p. 409–422, doi: 10.1007/BF00236999.
- ORR, P.J., BRIGGS, D.E.G., AND KEARNS, S.L., 1998, Cambrian Burgess Shale animals replicated in clay minerals: Science, v. 281, p. 1173–1175.
- ORR, P.J., KEARNS, S.L., AND BRIGGS, D.E.G., 2009, Elemental mapping of exceptionally preserved "carbonaceous compression" fossils: Palaeogeography Palaeoclimatology Palaeoecology, v. 277, p. 1–8.
- ORR, P.J., KEARNS, S.L., AND BRIGGS, D.E.G., 2002, Backscattered electron imaging of fossils exceptionally-preserved as organic compressions: PALAIOS, v. 17, p. 110–117.
- PAGE, A., GABBOTT, S.E., WILBY, P.R., AND ZALASIEWICZ, J.A., 2008, Ubiquitous Burgess Shale-style "clay templates" in low-grade metamorphic mudrocks: Geology, v. 36, p. 855–858.
- PÁLFY, J. AND SMITH, P.L., 2000, Synchrony between Early Jurassic extinction, oceanic anoxic event, and the Karoo-Ferrar flood basalt volcanism: Geology, v. 28, p. 747–750, doi: 10.1130/0091-7613(2000)28<747:sbejeo>2.0.co;2.
- Paytan, A. and McLaughlin, K., 2007, The oceanic phosphorus cycle: Chemical Reviews, v. 107, p. 563–576.
- Paytan, A., Mearon, S., Cobb, K., and Kastner, M., 2002, Origin of marine barite deposits: Sr and S isotope characterization: Geology, v. 30, p. 747–750, doi: 10.1130/00 91-7613(2002)030<0747:oombds>2.0.co;2.
- PICKERILL, R.K., 1994, Exceptional fossil record; distribution of soft-tissue preservation through the Phanerozoic; discussion: Geology, v. 22, p. 183–184.
- PIEńkowski, G., Hodbod, M., and Ullmann, C.V., 2016, Fungal decomposition of terrestrial organic matter accelerated Early Jurassic climate warming: Scientific Reports, v. 6, p. 1–11, doi: 10.1038/srep31930.

- PORTER, S.M., 2004, Closing the phosphatization window: testing for the influence of taphonomic megabias on the pattern of small shelly fossil decline: PALAIOS, v. 19, p. 178–183, doi: 10.2307/3515851.
- Poulton, T.P. AND AITKEN, J.D., 1989, The Lower Jurassic phosphorites of southeastern British Columbia and terrane accretion to western North America: Canadian Journal of Earth Sciences, v. 26, p. 1612–1616, doi: 10.1139/e89-137.
- QIN, X., MÜLLER, R.D., CANNON, J., LANDGREBE, T.C.W., HEINE, C., WATSON, R.J., AND TURNER, M., 2012, The GPlates geological information model and markup language: Geoscientific Instrumentation, Methods and Data Systems, v. 1, p. 111–134.
- RAISWELL, R., BOTTRELL, S.H., DEAN, S.P., MARSHALL, J.D., CARR, A., AND HATFIELD, D., 2002, Isotopic constraints on growth conditions of multiphase calcite-pyrite-barite concretions in Carboniferous mudstones: Sedimentology, v. 49, p. 237–254.
- RAISWELL, R., NEWTON, R.J., BOTTRELL, S.H., COBURN, P.M., BRIGGS, D.E.G., BOND, D.P.G., AND POULTON, S.W., 2008, Turbidite depositional influences on the diagenesis of Beecher's Trilobite bed and the Hunsrück Slate: site of soft tissue pyritization: American Journal of Science, v. 308, p. 105–129.
- REX, G.M., 1986, Further experimental investigations on the formation of plant compression fossils: Lethaia, v. 19, p. 143–159, doi: 10.1111/j.1502-3931.1986.tb00 725.x.
- REX, G.M. AND CHALONER, W.G., 1983, The experimental formation of plant compression fossils: Palaeontology, v. 26, p. 231–252.
- RICHARDS, F.A. AND REDFIELD, A.C., 1953, A correlation between the oxygen content of sea water and the organic content of marine sediments: Deep Sea Research, v. 1, p. 279–281.
- RIEDIGER, C.L., 2002, Hydrocarbon source rock potential and comments on correlation of the Lower Jurassic Poker Chip Shale, west-central Alberta: Bulletin of Canadian Petroleum Geology, v. 50, p. 263–276, doi: 10.2113/50.2.263.
- RITSEMA, C.J. AND GROENENBERG, J.E., 1993, Pyrite oxidation, carbonate weathering, and gypsum formation in a drained potential acid sulfate soil: Soil Science Society of America Journal, v. 57, p. 968–976, doi: 10.2136/sssaj1993.03615995005700040015x.
- RÖHL, H.-J., SCHMID-RÖHL, A., OSCHMANN, W., FRIMMEL, A., AND SCHWARK, L., 2001, The Posidonia Shale (lower Toarcian) of SW-Germany: an oxygen-depleted ecosystem controlled by sea level and palaeoclimate: Palaeogeography, Palaeoclimatology, Palaeoecology, v. 169, p. 273–299.
- Ross, D.J.K. AND BUSTIN, R.M., 2006, Sediment geochemistry of the Lower Jurassic Gordondale Member, northeastern British Columbia: Bulletin of Canadian Petroleum Geology, v. 54, p. 337–365, doi: 10.2113/gscpgbull.54.4.337.
- SAGEMANN, J., BALE, S.J., BRIGGS, D.E.G., AND PARKES, R.J., 1999, Controls on the formation of authigenic minerals in association with decaying organic matter: an experimental approach: Geochimica et Cosmochimica Acta, v. 63, p. 1083–1095, doi: 10.1016/S0016-7037(99)00087-3.
- SCHIFFBAUER, J.D., WALLACE, A.F., BROCE, J., AND XIAO, S., 2014a, Exceptional fossil conservation through phosphatization, in M. Laflamme, J.D. Schiffbauer, and S.A.F. Darroch (eds.), The Paleontological Society Papers, p. 59–82.
- SCHIFFBAUER, J.D., XIAO, S., CAI, Y., WALLACE, A.F., HUA, H., HUNTER, J., XU, H., PENG, Y., AND KAUFMAN, A.J., 2014b, A unifying model for Neoproterozoic-Palaeozoic exceptional fossil preservation through pyritization and carbonaceous compression: Nature Communications, v. 5, p. 1–12, doi: 10.1038/ncomms6754.
- Schiffbauer, J.D., Xiao, S., Sen Sharma, K., and Wang, G., 2012, The origin of intracellular structures in Ediacaran metazoan embryos: Geology, v. 40, p. 223–226.
- SCHLANGER, S. AND JENKYNS, H., 1976, Cretaceous oceanic anoxic events: causes and consequences: Geologie en Mijnbouw, v. 55, p. 179–184.
- Schulz, H.N., Brinkhoff, T., Ferdelman, T.G., Mariné, M.H., Teske, A., and Jørgensen, B.B., 1999, Dense populations of a giant sulfur bacterium in Namibian shelf sediments: Science, v. 284, p. 493–495.
- SCHULZ, H.N. AND SCHULZ, H.D., 2005, Large sulfur bacteria and the formation of phosphorite: Science, v. 307, p. 416-418.
- Schweigert, G., 2003, The lobster genus *Uncina* Quenstedt, 1851 (Crustacea: Decapoda: Astacidea: Uncinidae) from the Lower Jurassic: Stuttgarter Beitrage zur Naturkunde, v. 332, p. 1–43.
- Seilacher, A., 1970, Begriff und bedeutung der Fossil-Lagerstätten: Neues Jahrbuch für Geologie und Paläontologie, Monatshefte, v. 1970, p. 34–39.
- SEILACHER, A., 1982, Posidonia Shales (Toarcian, S. Germany): stagnant basin model revalidated, *in* E. Motanaro Gallitelli (ed.), Palaeontology, Essential of Historical Geology: STEM Mucci, Modena, Italy, p. 279–298.
- SEILACHER, A., 1990, Die Holzmadener Posidonienschiefer-Entstehung der Fossil-lagerstätte und eines Erdölmuttergesteins, in K.W. Weidert (ed.), Klassische Fundstellen der Paläontologie: Goldschneck-Verlag, Korb, Germany, p. 107–131.
- SEILACHER, A., REIF, W.-E., AND WESTPHAL, F., 1985, Sedimentological, ecological and temporal patterns of fossil Lagerstätten: Philosophical Transactions of the Royal Society of London, Biological Sciences, v. 311, p. 5–24.
- Sperling, E.A., 2017, Tackling the 99%: can we begin to understand the paleoecology of the small and soft-bodied animal majority?: The Paleontological Society Papers, v. 19, p. 77–86, doi: 10.1017/S1089332600002692.
- Sperling, E.A., Balthasar, U., and Skovsted, C.B., 2018, On the edge of exceptional preservation: insights into the role of redox state in Burgess Shale-type taphonomic windows from the Mural Formation, Alberta, Canada: Emerging Topics in Life Sciences, v. 2, p. 311–323, doi: 10.1042/etls20170163.

- Sperling, E.A., Carbone, C., Strauss, J.V., Johnston, D.T., Narbonne, G.M., and Macdonald, F.A., 2016, Oxygen, facies, and secular controls on the appearance of Cryogenian and Ediacaran body and trace fossils in the Mackenzie Mountains of northwestern Canada: Geological Society of America Bulletin, v. 128, p. 558–575, doi: 10.1130/b31329.1.
- SPERLING, E.A., WOLOCK, C.J., MORGAN, A.S., GILL, B.C., KUNZMANN, M., HALVERSON, G.P., MACDONALD, F.A., KNOLL, A.H., AND JOHNSTON, D.T., 2015, Statistical analysis of iron geochemical data suggests limited late Proterozoic oxygenation: Nature, v. 523, p. 451– 454, doi: 10.1038/nature14589.
- SPJELDNAES, N., 2002, Silurian bryozoans from Gotland fossilized in galena and sphalerite: GFF, v. 124, p. 27–33, doi: 10.1080/11035890201241027.
- STANKIEWICZ, B.A., BRIGGS, D.E.G., MICHELS, R., COLLINSON, M.E., FLANNERY, M.B., AND EVERSHED, R.P., 2000, Alternative origin of aliphatic polymer in kerogen: Geology, v. 28, p. 559–562.
- STRONACH, N.J., 1984, Depositional environments and cycles in the Jurassic Fernie Formation, southern Canadian Rocky Mountains, *in* D.F. Stott and D. Glass (eds.), The Mesozoic of Middle North America: A Selection of Papers from the Symposium on the Mesozoic of Middle North America: Canadian Society of Petroleum Geologists, Calgary, p. 43–68.
- SUAN, G., NIKITENKO, B.L., ROGOV, M.A., BAUDIN, F., SPANGENBERG, J.E., KNYAZEV, V.G., GLINSKIKH, L.A., GORYACHEVA, A.A., ADATTE, T., RIDING, J.B., FÖLLMI, K.B., PITTET, B., MATTIOLI, E., AND LÉCUYER, C., 2011, Polar record of Early Jurassic massive carbon injection: Earth and Planetary Science Letters, v. 312, p. 102–113, doi: 10.1016/j.epsl.2011.09.050.
- SUNBY, B., GOBEIL, C., SILVERBERG, N., AND MUCCI, A., 1992, The phosphorus cycle in coastal marine sediments: Limnology and Oceanography, v. 37, p. 1129–1145.
- Svensen, H., Planke, S., Chevallier, L., Malthe-Sørenssen, A., Corfu, F., and Jamtveit, B., 2007, Hydrothermal venting of greenhouse gases triggering Early Jurassic global warming: Earth and Planetary Science Letters, v. 256, p. 554–566, doi: 10.1016/j. epsl.2007.02.013.
- SZPAK, P., 2011, Fish bone chemistry and ultrastructure: implications for taphonomy and stable isotope analysis: Journal of Archaeological Science, v. 38, p. 3358–3372, doi: 10.1016/j.jas.2011.07.022.
- Takashima, R., Nishi, H., Huber, B.T., and Leckie, R.M., 2006, Greenhouse world and the Mesozoic ocean: Oceanography, v. 19, p. 82–92, doi: 10.5670/oceanog.2006.07.
- TARHAN, L.G., DROSER, M.L., PLANAVSKY, N.J., AND JOHNSTON, D.T., 2015, Protracted development of bioturbation through the early Palaeozoic Era: Nature Geoscience, v. 8, p. 865–869, doi: 10.1038/ngeo2537.
- Them, T.R., Gill, B.C., Caruthers, A.H., Gerhardt, A.M., Gröcke, D.R., Lyons, T.W., Marroquín, S.M., Nielsen, S.G., Trabucho Alexandre, J.P., and Owens, J.D., 2018, Thallium isotopes reveal protracted anoxia during the Toarcian (Early Jurassic) associated with volcanism, carbon burial, and mass extinction: Proceedings of the National Academy of Sciences, v. 115, p. 6596–6601, doi: 10.1073/pnas.1803478115.
- THEM, T.R., GILL, B.C., CARUTHERS, A.H., GROCKE, D.R., TULSKY, E.T., MARTINDALE, R.C., POULTON, T.P., AND SMITH, P.L., 2017a, High-resolution carbon isotope records of the Toarcian Oceanic Anoxic Event (Early Jurassic) from North America and implications for the global drivers of the Toarcian carbon cycle: Earth and Planetary Science Letters, v. 459, p. 118–126, doi: 10.1016/j.epsl.2016.11.021.

- THEM, T.R., GILL, B.C., SELBY, D., GRÖCKE, D.R., FRIEDMAN, R.M., AND OWENS, J.D., 2017b, Evidence for rapid weathering response to climatic warming during the Toarcian Oceanic Anoxic Event: Scientific Reports, v. 7, p. 1–10, doi: 10.1038/s41598-017-05307-y.
- VALENTINE, J.W., 1989, How good was the fossil record? Clues from the Californian Pleistocene: Paleobiology, v. 15, p. 83–94.
- van Gemerden, H., 1993, Microbial mats: a joint venture: Marine Geology, v. 113, p. 3–25, doi: 10.1016/0025-3227(93)90146-M.
- Waloszek, D., 2003, The "Orsten" window—a three-dimensionally preserved upper Cambrian meiofauna and its contribution to our understanding of the evolution of Arthropoda: Paleontological Research, v. 7, p. 71–88.
- WATABE, N. AND PAN, C.-M., 1984, Phosphatic shell formation in atremate brachiopods: American Zoologist, v. 24, p. 977–985.
- Watson, A.J., Lenton, T.M., and Mills, B.J.W., 2017, Ocean deoxygenation, the global phosphorus cycle and the possibility of human-caused large-scale ocean anoxia: Philosophical Transactions, Series A, Mathematical, Physical, and Engineering Sciences, v. 375, p. 1–14, doi: 10.1098/rsta.2016.0318.
- Wilby, P.R., 1993, The role of organic matrices in post-mortem phosphatization of soft-tissues: Kaupia, Darmstaedter Beitraeger zur Naturgeschichte, v. 2, p. 99–113.
- WILBY, P.R. AND WHYTE, M.A., 1995, Phosphatized soft tissues in bivalves from the Portland Roach of Dorset (Upper Jurassic): Geological Magazine, v. 132, p. 117–120.
- WILLIAMS, A. AND HOLMER, L.E., 1992, Ornamentation and shell structure of acrotretoid brachiopods: Palaeontology, v. 35, p. 657–692.
- WILLIAMS, A., MACKAY, S., AND CUSACK, M., 1992, Structure of the organophosphatic shell of the brachiopod *Discina*: Philosophical Transactions, Biological Sciences, v. 337, p. 83–104.
- WILLIAMS, M., BENTON, M.J., AND ROSS, A., 2015, The Strawberry Bank Lagerstätte reveals insights into Early Jurassic life: Journal of the Geological Society, v. 172, p. 683–692, doi: 10.1144/jgs2014-144.
- WRIGHT, N., ZAHIROVIC, S., MÜLLER, R.D., AND SETON, M., 2013, Towards community-driven paleogeographic reconstructions: integrating open-access paleogeographic and paleobiology data with plate tectonics: Biogeosciences, v. 10, p. 1529–1541, doi: 10.51 94/bg-10-1529-2013.
- XIAO, S. AND KNOLL, A.H., 1999, Fossil preservation in the Neoproterozoic Doushantuo phosphorite Lagerstätte, South China: Lethaia, v. 32, p. 219–240.
- XIAO, S. AND SCHIFFBAUER, J.D., 2009, Microfossil phosphatization and its astrobiological implications, in J. Seckbach and M. Walsh (eds.), From Fossils to Astrobiology: Record of Life on Earth and Search for Extraterrestrial Biosignatures: Springer Netherlands, p. 89–117
- ZABINI, C., SCHIFFBAUER, J.D., XIAO, S., AND KOWALEWSKI, M., 2012, Biomineralization, taphonomy, and diagenesis of Paleozoic lingulide brachiopod shells preserved in silicified mudstone concretions: Palaeogeography, Palaeoclimatology, Palaeoecology, v. 326–328, p. 118–127.
- ZHANG, Y., YIN, L., XIAO, S., AND KNOLL, A.H., 1998, Permineralized fossils from the terminal Proterozoic Doushantuo Formation, South China: Journal of Paleontology, v. 72 (supplement to no. 4), p. 1–52.

Received 24 May 2019; accepted 15 September 2019.